

## Interplay of channels, pumps and organelle location in calcium microdomain formation

Martin Peglow<sup>1,3</sup>, Barbara A Niemeyer<sup>2</sup>, Markus Hoth<sup>2</sup>  
and Heiko Rieger<sup>1,3</sup>

<sup>1</sup> Theoretical Physics, Saarland University, D-66041 Saarbrücken, Germany

<sup>2</sup> Department of Biophysics, Saarland University, D-66424 Homburg, Germany

E-mail: [mape@lusi.uni-sb.de](mailto:mape@lusi.uni-sb.de) and [h.rieger@mx.uni-saarland.de](mailto:h.rieger@mx.uni-saarland.de)

*New Journal of Physics* **15** (2013) 055022 (27pp)


Received 4 October 2012

Published 24 May 2013

Online at <http://www.njp.org/>

doi:10.1088/1367-2630/15/5/055022

**Abstract.** To analyze the influence of  $\text{Ca}^{2+}$  microdomains on the global cytosolic  $\text{Ca}^{2+}$  concentration, we consider the polarization and activation of T-cells after the formation of an immunological synapse as a model system. For T-cell proliferation and activation, a high and robust  $\text{Ca}^{2+}$  signal lasting from minutes up to hours is needed. This raises the intriguing question of how T-cells overcome all those mechanisms which normally remove an increased  $\text{Ca}^{2+}$  level as fast as possible from the cytosol. With the help of theoretical models we predict that, after the formation of a local  $\text{Ca}^{2+}$  influx pathway via STIM1 and Orai1, mitochondria relocation toward and accumulation of plasma membrane  $\text{Ca}^{2+}$  ATPase and sarcoplasmic/ endoplasmic reticulum calcium ATPase pumps at the immunological synapse are sufficient to achieve a long-lasting increased global  $\text{Ca}^{2+}$  concentration. In addition, we also uncover new mechanisms to generate  $\text{Ca}^{2+}$  oscillations, which are important for efficient T-cell activation. Experimental tests and the implications of our predictions are discussed.

 Online supplementary data available from [stacks.iop.org/NJP/15/055022/mmedia](http://stacks.iop.org/NJP/15/055022/mmedia)

<sup>3</sup> Authors to whom any correspondence should be addressed.



Content from this work may be used under the terms of the [Creative Commons Attribution-NonCommercial-ShareAlike 3.0 licence](http://creativecommons.org/licenses/by-nc-sa/3.0/). Any further distribution of this work must maintain attribution to the author(s) and the title of the work, journal citation and DOI.

**Contents**

<b>1. Introduction</b>	<b>2</b>
<b>2. Ca<sup>2+</sup> release-activated Ca<sup>2+</sup> channel formation</b>	<b>5</b>
2.1. The stochastic reaction–diffusion model	5
2.2. Results I	7
<b>3. One-dimensional model for the effect of mitochondria relocation on Ca<sup>2+</sup> signals</b>	<b>9</b>
3.1. Stationary Ca <sup>2+</sup> concentration profile	10
3.2. Parameter choice	11
3.3. Results	12
<b>4. Ca<sup>2+</sup> signaling during T-cell activation and polarization</b>	<b>14</b>
4.1. Microdomains and global Ca <sup>2+</sup> during T-cell polarization	14
4.2. The three-dimensional full cell reaction–diffusion model	14
4.3. Parameter values	17
4.4. Results	18
<b>5. Discussion</b>	<b>23</b>
<b>Acknowledgments</b>	<b>25</b>
<b>References</b>	<b>25</b>

**1. Introduction**

Calcium (Ca<sup>2+</sup>) is a versatile and ubiquitous diffusive messenger in nearly all cells [1]. Calcium signaling controls processes as diverse as gene expression, muscle contraction, fertilization, proliferation, development, learning and memory. However, how these very specific outcomes are encoded and modulated by the magnitude and/or the spatial and temporal patterns of Ca<sup>2+</sup> signals is largely unknown. Besides the information content that can be obtained by the amplitude or the kinetics and frequency of Ca<sup>2+</sup> waves or oscillations, the presence of Ca<sup>2+</sup> microdomains, local high Ca<sup>2+</sup> concentrations, can create high specificity. It is known that these Ca<sup>2+</sup> microdomains control, for example, neuronal function [2, 3], muscle contraction and gene expression [4, 7].

The physical origin of the variety of calcium (Ca<sup>2+</sup>) signals is the interplay of channels and pumps that transfer Ca<sup>2+</sup> between different cellular compartments (including the extracellular space), either by simple diffusion along concentration gradients (channels) or by active processes involving ATP<sup>4</sup> as an energy source (active transporters and pumps). The capacities of these channels and pumps depend nonlinearly on Ca<sup>2+</sup> concentration, giving rise to positive and negative feedback loops that generate interesting spatio-temporal dynamics comprising spikes, oscillations, waves, etc that have been studied for several decades now (for an overview of the physics of calcium signals see [5]). Much less is known about the conditions under which specific spatial arrangements of channels, pumps and organelles lead to the formation of Ca<sup>2+</sup> microdomains, i.e. pronounced spatial inhomogeneities in the Ca<sup>2+</sup> concentrations. This is what we are going to study in this paper within the context of T-cell polarization.

<sup>4</sup> *Frequently used abbreviations.* ATP: adenosine tri-phosphate; CRAC: Ca<sup>2+</sup> release-activated Ca<sup>2+</sup> channel; ER: endoplasmic reticulum; IP<sub>3</sub>: inositol-1,4,5-trisphosphate; IS: immunological synapse; PM: plasma membrane; PMCA: plasma membrane Ca<sup>2+</sup> ATPase; SERCA: sarcoplasmic/endoplasmic reticulum calcium ATPase; STIM: stromal interaction molecule.

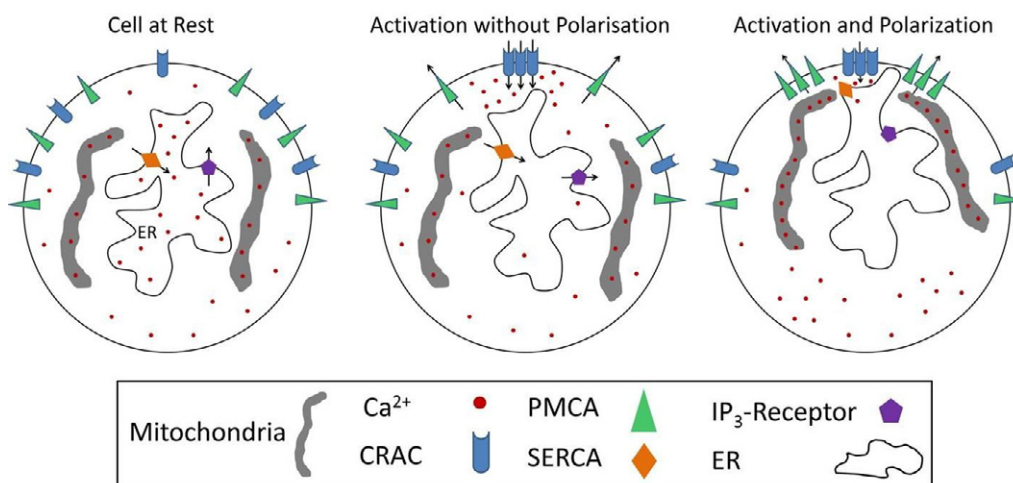


**Figure 1.** Schematic presentation of Ca<sup>2+</sup> signaling and polarization in T-cells. From left to right, three different situations are shown: (i) The cell at rest. (ii) Activation without polarization. This situation can be obtained in particular experiments where due to experimental constraints CRAC channels are activated but no pump or organelle relocation occurred. (iii) Activation with polarization. Under physiological conditions T-cell activation is accompanied by relocation of channels, pumps, mitochondria and the ER.

For the activation of T-cells, which is very important for human immune defense, the occurrence and formation of Ca<sup>2+</sup> microdomains is essential. After the formation of an immunological synapse (IS), the stable junction or contact area between the T-cell and an antigen-presenting cell, T-cell activation is initiated. The crucial step for successful activation, following the IS formation, is a high and robust Ca<sup>2+</sup> signal, emerging from a directed Ca<sup>2+</sup> influx across the plasma membrane (PM) through the gating of the store operated Ca<sup>2+</sup> release-activated Ca<sup>2+</sup> (CRAC) channel [6]. These special signals of high intracellular calcium last from several minutes even up to hours. An intriguing question is how are T-cells, in this situation, able to overcome all those mechanisms that nature had provided to remove an increased cytosolic Ca<sup>2+</sup> as fast as possible, since under normal circumstances high cytosolic Ca<sup>2+</sup> concentrations are lethal to the cell.

A closer look at the various processes involved reveals the importance of Ca<sup>2+</sup> microdomain regulation during the activation process: the formation of the IS is paralleled by a cell polarization, which involves the re-localization of cell organelles, Ca<sup>2+</sup> channels and pumps and as a consequence leads to a specific spatial organization of Ca<sup>2+</sup> signals (see figure 1). The key players that induce the polarization and generation of Ca<sup>2+</sup> signals in T-cells are: (i) CRAC channels, which are the main Ca<sup>2+</sup> source in T-cells; (ii) plasma membrane Ca<sup>2+</sup> ATPase (PMCA) pumps, which are located in the cell's PM and pump the Ca<sup>2+</sup> from the cytosol back into the extracellular space; (iii) endoplasmic reticulum (ER), which is the main intracellular Ca<sup>2+</sup> store with its IP<sub>3</sub> receptors to release Ca<sup>2+</sup> and the SERCA pumps to pump Ca<sup>2+</sup> back into the ER; (iv) mitochondria, which can act not only as strong Ca<sup>2+</sup> sinks, but also as Ca<sup>2+</sup> distributors.

CRAC channels, the main Ca<sup>2+</sup> entry pathway in T-cells, are store operated channels and are activated by Ca<sup>2+</sup> depletion of the ER. Under physiological conditions the ER depletion

is triggered by an external stimulus resulting in the production of  $\text{IP}_3$  and  $\text{Ca}^{2+}$  release by  $\text{IP}_3$  receptors. CRAC channels are inactivated or at least inhibited by  $\text{Ca}^{2+}$  in different ways [8–10]. Refilling of the  $\text{Ca}^{2+}$  store ER, which occurs when the global  $\text{Ca}^{2+}$ -concentration rises and SERCA pumps are activated, is one mechanism to end CRAC channel activation. Apart from that, the channel is also deactivated by a  $\text{Ca}^{2+}$  microdomain in the close vicinity of the channel pore. At least two independent and  $\text{Ca}^{2+}$ -controlled negative feedback mechanisms of CRAC channel inhibition exist [11–13]. Nevertheless, a sustained  $\text{Ca}^{2+}$  influx of up to several hours can be measured and is crucial for T-cell activation as well as other T-cell functions including transcription and proliferation. It has been hypothesized that mitochondria have to be close to CRAC channels, thereby decreasing the  $\text{Ca}^{2+}$  microdomain right at the channel and preventing part of the  $\text{Ca}^{2+}$ -dependent CRAC channel inactivation [6, 14]. This leads to enhanced CRAC activity and finally to increased cytosolic  $\text{Ca}^{2+}$  concentration. Besides the mitochondria relocation, recent work has shown that PMCA pumps also redistribute during T-cell polarization and accumulate near mitochondria at the IS [15]. Whether this pump accumulation at the IS is necessary for T-cell activation remains an open question. In addition to the accumulation of mitochondria near the CRAC channel, it is also known that a physical and functional coupling between mitochondria and the ER exists (for a review see [16]) and is also expected to play an important role during the T-cell activation.

A number of theoretical works have focused on the modulation of calcium release through  $\text{IP}_3$  receptors by  $\text{Ca}^{2+}$  buffers [17–19]. Since this well-studied  $\text{Ca}^{2+}$  channel has activating and, in particular, inhibitory  $\text{Ca}^{2+}$ -binding sites,  $\text{Ca}^{2+}$  buffers can promote prolonged opening times of the channel, leading to an increased  $\text{Ca}^{2+}$  flux from the ER into the cytosol. The CRAC channel, which in our system is the main  $\text{Ca}^{2+}$  source, displays similar  $\text{Ca}^{2+}$ -induced inactivation effects, partly store-dependent and partly independent, and these effects are also modulated by  $\text{Ca}^{2+}$  buffers [9, 10]. One might speculate that the relocation of mitochondria toward the IS during T-cell activation just inhibits the  $\text{Ca}^{2+}$ -induced inactivation of CRAC channels by buffering the intruding  $\text{Ca}^{2+}$ . For this to happen the mitochondria must be very close to a putative inhibitory  $\text{Ca}^{2+}$  site of the CRAC channel, for which experimental evidence is lacking. Simultaneously with mitochondria relocation one observes a PMCA pump accumulation at the IS during T-cell activation [15]. Therefore we propose here a role for mitochondria that has not been studied so far, namely to absorb intruding  $\text{Ca}^{2+}$  before it reaches nearby PMCA (and also SERCA) pumps and release it far away from the plasma membrane deep inside the cell body.

A quantitative understanding of the interplay of the spatial arrangement of  $\text{Ca}^{2+}$  storing or redistributing organelles as well as  $\text{Ca}^{2+}$  channels and pumps leading to specific long-lasting  $\text{Ca}^{2+}$  signaling patterns is still lacking. Early modeling attempts took the  $\text{Ca}^{2+}$  buffering capability of mitochondria into account ([20, 21], for a review see [22]) and found them to be an important factor in the amplitude regulation of intracellular  $\text{Ca}^{2+}$  oscillations. These compartment models assume a spatially homogeneous cytosolic  $\text{Ca}^{2+}$  concentration, neglect  $\text{Ca}^{2+}$  diffusion and the build-up of  $\text{Ca}^{2+}$  micro-domains via specific spatial arrangements of  $\text{Ca}^{2+}$  sources and sinks—and thus are not suited to address the questions we are interested in: to understand the complex correlation between the spatial redistribution of organelles and channels/pumps and the resulting formation of local (microdomains) and global (cytosolic)  $\text{Ca}^{2+}$  signals, which in the end lead to a sustained increase in  $\text{Ca}^{2+}$  concentration during the T-cell activation. To the best of our knowledge, we present for the first time a model to investigate how the spatial arrangement of and the distances between the different cell organelles influence the  $\text{Ca}^{2+}$  signals in cells.

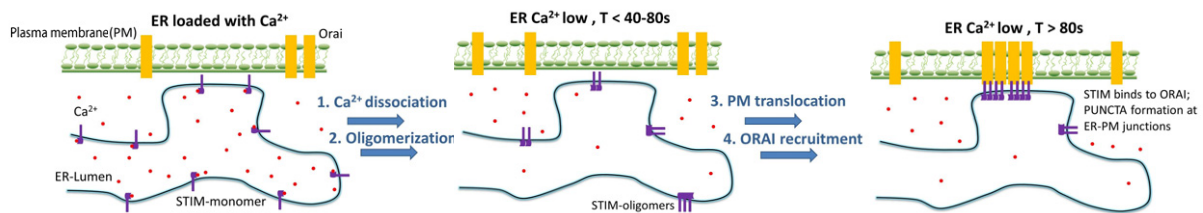


**Figure 2.** Four steps of the STIM1-to-ER pathway. If the ER is loaded the  $\text{Ca}^{2+}$  binding to STIM1 prevents the oligomerization of the protein. In a first activation step, receptor-induced  $\text{Ca}^{2+}$  release leads to  $\text{Ca}^{2+}$  dissociation from STIM1 and thus to fast oligomerization. Oligomer diffusion is followed by an accumulation of STIM1 at ER–PM junctions where the interaction with the PM  $\text{Ca}^{2+}$  channel Orai1 leads to CRAC channel formation and  $\text{Ca}^{2+}$  influx. Inspired by Liou *et al* [26].

The paper is organized as follows. In section 2 we formulate a mathematical model to understand the assembly of functional CRAC channels. Section 3 contains the analysis of a simplified one-dimensional (1D) model through which the influence of mitochondria-relocation toward the IS on global  $\text{Ca}^{2+}$  concentration is demonstrated. In section 4 we present a physiologically more realistic three-dimensional (3D) model to analyze the influence of the distance between mitochondria and the IS on global and local  $\text{Ca}^{2+}$  concentrations and the effect of different PMCA distributions and the ER/SERCA location. Section 5 contains a discussion and some open questions.

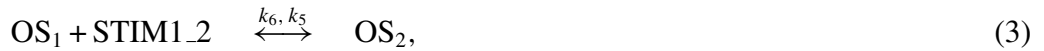
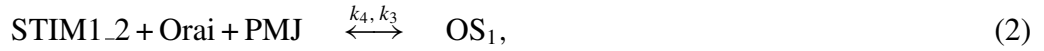
## 2. $\text{Ca}^{2+}$ release-activated $\text{Ca}^{2+}$ channel formation

The functional store operated CRAC channel arises from the interaction of the two proteins STIM1 (stromal interaction molecule) and Orai1, and it has been shown that a direct interaction between these two proteins is sufficient to open the Orai1 channel pore [23–25]. The signaling pathway of STIM1 ER-to-PM, which is responsible for local  $\text{Ca}^{2+}$  signals and high cytosolic concentration gradients, can be explained by a sequence of four steps [26]. STIM1 is located in the ER plasma membrane (PM) and senses  $\text{Ca}^{2+}$  by a  $\text{Ca}^{2+}$ -binding site in the lumen of the ER [27]. The depletion of the ER  $\text{Ca}^{2+}$  stores leads to  $\text{Ca}^{2+}$  dissociation from the luminal  $\text{Ca}^{2+}$ -binding site and then to a fast oligomerization or dimerization of STIM1 monomers (see figure 2). This oligomerization process lasts about 5 s [26] and is followed by a diffusion of these STIM1 dimers to the cell PM. At the so-called plasma membrane junctions (PMJ), which are locations where the distance between the ER and the cell PM is smaller than 20 nm, STIM1 dimers catch Orai1 tetramers diffusing in the cell PM. This interaction of STIM1 with the  $\text{Ca}^{2+}$  channel Orai1 then leads to a strong and directed  $\text{Ca}^{2+}$  flux into the cell.

### 2.1. The stochastic reaction–diffusion model

We formulate a theoretical model with which we want to study the formation of local STIM1/Orai1 hotspots responsible for store operated  $\text{Ca}^{2+}$  influx. A related model was introduced in [28] to understand the experimentally observed influence of STIM1 mutants upon  $\text{Ca}^{2+}$  influx; here we focus on its physical aspects. Assuming an already depleted  $\text{Ca}^{2+}$  store,

steps 2–4 of the STIM1 ER-to-PM pathway (see figure 2) are described by the following reaction scheme:



Reaction (1) represents the STIM1 dimerization, where STIM1<sub>2</sub> denotes the STIM1 dimer; (2) represents the binding of a STIM1 dimer to Orai1 at a PM junction (PMJ), resulting in a first open CRAC channel state OS<sub>1</sub>. Reactions (3) and (4) represent subsequent recruitment of more STIM1 dimers to an existing channel, each binding of an additional STIM1 dimer to an open channel OS<sub>n</sub> yielding a channel state OS<sub>n+1</sub> with higher capacity. Each of these four states contributes in a specific, pre-defined way to the total CRAC channel current

$$I_{\text{CRAC}} = 0.001 \text{OS}_1 + 0.025 \text{OS}_2 + 0.275 \text{OS}_3 + 1.0 \text{OS}_4, \quad (6)$$

modeling the experimentally observed graded channel currents [32, 33].

The on-rates  $k_3$ ,  $k_5$ ,  $k_7$  and  $k_9$  as well as the off-rates  $k_4$ ,  $k_6$ ,  $k_8$  and  $k_{10}$  are not assumed to be independent, since the STIM1 to Orai1 binding process is less probable when more STIM1 dimers are already bound to an Orai1 tetramer (negative cooperativity). Similarly, the CRAC channel states are more stable when more STIM1 dimers participate in forming the channel. This cooperativity is controlled by the cooperativity factors  $\alpha$  and  $\beta$  by assuming that

$$k_{2n+3} = \alpha^n k_3, \quad k_{2n+4} = \beta^n k_4 \quad \text{for } n \in \{0, 1, 2, 3\}, \quad (7)$$

where negative cooperativity means  $0 < \alpha, \beta < 1$ .

STIM1 diffuses on the ER surface, and Orai1 in the PM, and the CRAC channels OS<sub>1</sub>–OS<sub>4</sub> and PM junctions are assumed to be stationary. In our Monte Carlo algorithm the STIM and Orai particles undergo a random walk and the diffusion events are treated as reactions with reaction rates  $d_i = D_i/\Delta x$  where  $i \in \{\text{STIM1}, \text{STIM1}_2, \text{Orai}\}$ .

We discretize the diffusion process in the following way: the CRAC channel formation is a local process, meaning that the recruitment length for STIM1 reaching a certain PMJ is very small [26]. With knowledge of the diffusion constant  $D_{\text{STIM1}} = 0.05\text{--}0.1 \mu\text{m}^2 \text{s}^{-1}$  of STIM1/STIM1<sub>2</sub> and the time period required for STIM1 to accumulate at the PMJ ( $t \approx 40$  s), one can calculate the average recruitment length for STIM1 as  $\langle x_{\text{recruit}} \rangle = (4Dt/\pi)^{1/2} = 1.6\text{--}2.3 \mu\text{m}$  [31]. Therefore we model an area of  $15 \times 15$  grid cells, each of  $\Delta x^2 = (0.2 \mu\text{m})^2$  size. This  $9 \mu\text{m}^2$  area represents the cell PM and the ER membrane at the same time with a unique grid cell right in the middle of the geometry, labeled as the PMJ (see figure 3(a)). We assume periodic boundary conditions for the diffusion of STIM1, STIM1<sub>2</sub> and Orai1 and we restrict a STIM1–Orai1 interaction (reactions/equations (2)–(4)) to the PMJ grid cell. At the PMJ, STIM1 dimers can trap Orai1 and build up the four different CRAC channel states OS<sub>1</sub>, OS<sub>2</sub>, OS<sub>3</sub> and OS<sub>4</sub> ( $D_{\text{OS}_i} = 0 \mu\text{m}^2 \text{s}^{-1}$ ,  $i = 1, 2, 3, 4$ ), consisting of one Orai1 tetramer and one to four STIM1 dimers. The whole model setup is sketched in figure 3(b).

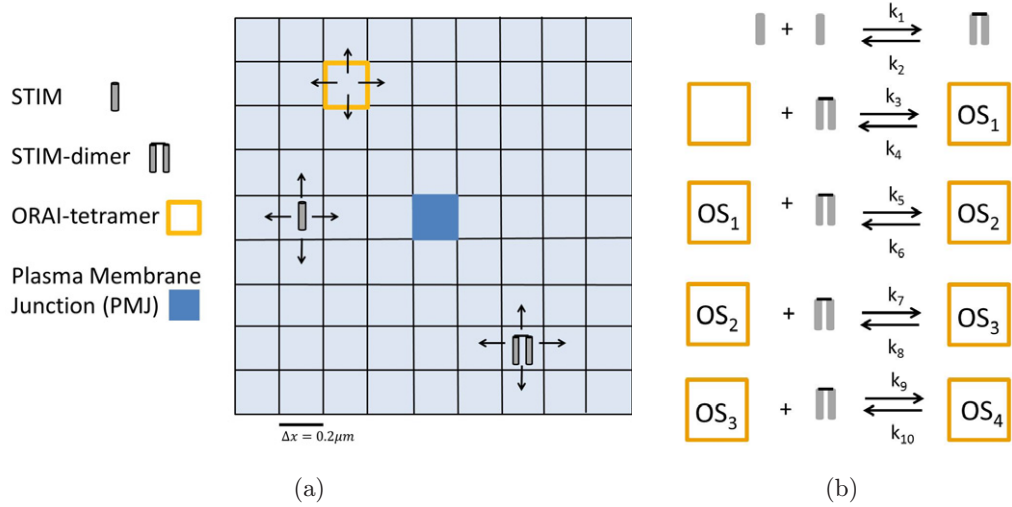


**Figure 3.** Sketch of the two-dimensional (2D) reaction–diffusion model for CRAC channel formation via STIM1–Orai1 interaction. (a) Model geometry: the square lattice represents simultaneously the plasma membrane (in which STIM1 and STIM1 dimers diffuse) and the ER membrane (in which Orai1 tetramers diffuse). The PMJ is immobile. (b) Reaction scheme for STIM1 dimerization and CRAC channel ( $OS_1, \dots, OS_4$ ) formation.

**Table 1.** Reaction and diffusion rates used as the Base Case scenario of the stochastic two-dimensional model.

Species	$D$ ( $\mu\text{m}^2 \text{s}^{-1}$ )	Reaction rate	
STIM1	0.1 [26]	$k_3$	$k_{\text{on}}$
STIM1 <sub>2</sub>	0.05 [26]	$k_5$	$k_{\text{on}}\alpha$
Orai1	0.07 [25]	$k_7$	$k_{\text{on}}\alpha^2$
$OS_1, OS_2, OS_3, OS_4$	0	$k_9$	$k_{\text{on}}\alpha^3$
Reaction	–Rate	$k_4$	$k_{\text{off}}$
$k_{\text{on}}$	$1.5 \times 10^8$ ( $1 \text{ Ms}^{-1}$ )	$k_6$	$k_{\text{off}}\beta$
$k_{\text{off}}$	0.8 ( $1 \text{ s}^{-1}$ )	$k_8$	$k_{\text{off}}\beta^2$
$k_1$	$10^8$ ( $1 \text{ Ms}^{-1}$ )	$k_{10}$	$k_{\text{off}}\beta^3$
$k_2$	0.05 ( $1 \text{ s}^{-1}$ )	Number of STIM1 monomers	6000

We analyze this two-dimensional (2D) reaction–diffusion system by performing computer simulations using a Gillespie Monte Carlo algorithm [29] implemented with efficient techniques to optimize the computation time [30]. At the start of our simulation at time  $t = 0$ , we homogeneously distribute all Orai1 and STIM1 particles in the cell PM and the ER, respectively. The parameters (reaction rates and diffusion constants) of our Base Case scenario are shown in table 1 and we indicate whether they differ.

## 2.2. Results I

In figure 4(a) we show the temporal evolution of a CRAC current  $I_{\text{CRAC}}$  that results in the formation of an Orai1 channel hotspot at the PMJ, assuming our Base Case parameters.

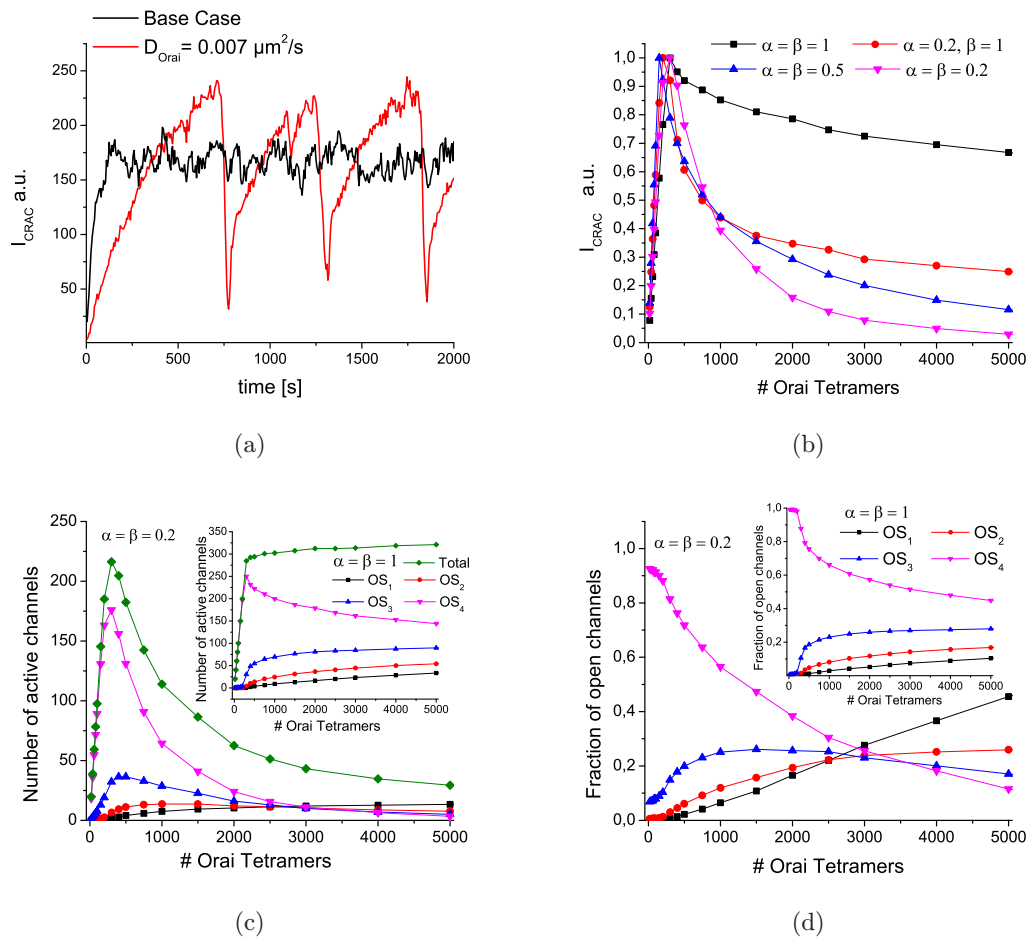


**Figure 4.** (a) Temporal evolution of CRAC current. Black curve indicates the Base Case scenario and the oscillating red curve is obtained for a slower Orail1 diffusion additionally to unbinding of STIM1 monomers instead of dimers. (b) Normalized CRAC currents as a function of Orail1 expression for different values of the cooperativity factors  $\alpha$  and  $\beta$ . (c) Number of active channels as a function of Orail1 expression. (d) Composition of channel population as a function of Orail1 expression.

Very interestingly, our model predicts oscillations of the CRAC current  $I_{CRAC}$  which can possibly enhance the efficiency of  $\text{Ca}^{2+}$  signals in T-cells. These oscillations can only be obtained if the following three conditions hold simultaneously: decreased Orail1 diffusion, with the diffusion constant  $D_{Orai1}$  determining the oscillation period; negative cooperativity of binding and dissociation ( $\alpha = \beta < 1$ ); and a slightly altered reaction scheme, which assumes dissociation of two STIM1 monomers instead of dissociation of one STIM1 dimer. Under these conditions, the OS<sub>4</sub> state dominates and if a dissociation process takes place two STIM1 monomers are created. These STIM1 monomers first have to dimerize again and diffuse back to the PMJ area in order to trap Orail1 tetramers or to build up new channel states. After the first oscillation period, the Orail1 density at the PMJ is increased because of the slower Orail1 diffusion and the CRAC channel formation starts again. Assuming a faster STIM1 oligomerization (higher reaction rate  $k_1$ , data not shown) no oscillations occur. In this case



the dimerization at the PMJ is more probable than a STIM1 monomer diffusion event out of the PMJ grid cell and the result does not differ from the Base Case scenario with STIM1 dimer dissociation.

As a further result, our model predicts STIM1 to Orai1 binding with a negative ( $\alpha < 1$ ) cooperativity as well as a STIM1 dissociation with a negative ( $\beta < 1$ ) cooperativity to be essential for CRAC channel formation and currents. Otherwise, assuming that STIM1 to Orai1 binding is independent and noncooperative ( $\alpha = 1$ ), the model cannot account for the experimentally found  $I_{\text{CRAC}}$  versus Orai1 relation [32]. For a fixed number of STIM1 proteins the current first increases with increasing number of Orai1 tetramers until an optimal STIM1-Orai1 ratio is reached. Past this optimal ratio, which for our model is  $\text{STIM1/Orai1} = 7.5$ , the CRAC current decreases with stronger Orai1 expression until  $I_{\text{CRAC}}$  is nearly zero, as was observed experimentally in [32].

Our model only reproduces this current versus Orai1 expression, mainly the zero current for Orai1 overexpression, with a negative cooperativity ( $\alpha < 1$ ) of binding as well as a negative cooperativity ( $\beta < 1$ ) of dissociation (see figure 4(b)). The effect of this negative cooperativity on the CRAC current is shown in figures 4(c) and (d), where we plotted the number of active channels and the fraction of different channel states  $\text{OS}_1\text{--OS}_4$  as a function of Orai1 expression. For a small number of Orai1 tetramers the large number of STIM1 proteins (6000 STIM1 monomers) overcomes the negative cooperativity of binding and nearly all the available Orai1 channels are in the  $\text{OS}_4$  state, which delivers the major part of the total CRAC current (see equation (6)). But for larger STIM1:Orai1 ratios and a value of  $\alpha < 1$  the STIM1 dimers start to bind to Orai1 more homogeneously. First, the channel state  $\text{OS}_4$  will dominate the current, but at a value of about 3000 Orai1 tetramers there exists a crossover above which the state  $\text{OS}_1$  will dominate, followed by the states  $\text{OS}_2$  and  $\text{OS}_3$ . For noncooperative binding and dissociation the channel state  $\text{OS}_4$  will, independent of Orai1 expression levels, always dominate the CRAC current. As Orai1 channels in the  $\text{OS}_4$  state contribute most strongly to the CRAC current, the negative cooperativity of binding/dissociation is needed to account for the inactivating currents at high Orai1 levels.

### 3. One-dimensional model for the effect of mitochondria relocation on $\text{Ca}^{2+}$ signals

In this section we want to understand qualitatively the effect of mitochondria relocation within the cytosol on the spatial distribution of  $\text{Ca}^{2+}$  distribution in the presence of opened CRAC channels. The situation we envisage is one in which the CRAC channel has already formed (see section 2) and the ER is depleted and stays depleted (experimentally realizable by the blockage of SERCA pumps via Tapsigargin). This means we have a constant influx of  $\text{Ca}^{2+}$  into the cell through CRAC channels and out of the cell through PMCA. The question is whether the location of mitochondria *within* the cell has an influence on the emerging total  $\text{Ca}^{2+}$  content in the cell.

To provide a first insight we reduced the system to one spatial dimension, i.e. a single variable  $x$  varying between  $x = 0$  (position of the IS with activated CRAC channels) and  $x = L$  (position opposite the IS, the location of PMCA pumps). Mitochondria occupy the region between  $x_{\text{in}}$  and  $x_{\text{out}}$ , and for simplicity we assume that the whole  $\text{Ca}^{2+}$  absorption capacity of the mitochondria is focused at position  $x_{\text{in}}$  and all the  $\text{Ca}^{2+}$  absorbed at  $x_{\text{in}}$  is re-injected at position  $x_{\text{out}}$ . It is straightforward to generalize the model to continuous distributions of sources and sinks—here we stick to the simplest version since it is sufficient for understanding the basic mechanisms. In [15], a related model was studied numerically with additional PMCA pumps at

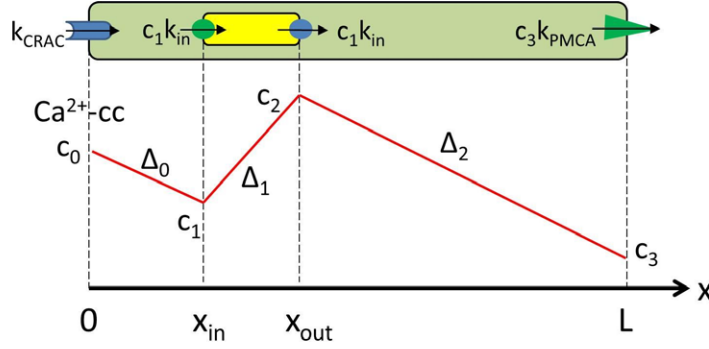


**Figure 5.** (Top) Sketch of the 1D model for mitochondria relocation: cytosol is light green, mitochondria are yellow,  $\text{Ca}^{2+}$  sources (CRAC and mitochondria) are blue and  $\text{Ca}^{2+}$  sinks (mitochondria and PMCA) are green. (Bottom) Expected spatial dependence of  $\text{Ca}^{2+}$  concentration.  $c_0$  is the concentration at the location of the CRAC channel ( $x = 0$ ),  $c_1$  at the front end of the mitochondria ( $x = x_{\text{in}}$ ),  $c_2$  at the back end ( $x = x_{\text{out}}$ ) and  $c_3$  at the PMCA pumps ( $x = L$ ). The slopes of the linear pieces are denoted as  $\Delta_0$ ,  $\Delta_1$  and  $\Delta_2$  (see the text).

the IS position  $x = 0$ . Here we discuss a simpler version that is analytically solvable. The model and the expected spatial dependence of the  $\text{Ca}^{2+}$  concentration are sketched in figure 5.

Moreover, we assume that cytosolic  $\text{Ca}^{2+}$  is freely diffusing (i.e. no mobile buffers present) with sources and sinks of given strength as described above. Mathematically, this problem is described by the 1D diffusion equation

$$\frac{\partial c(x, t)}{\partial t} = D \frac{\partial^2 c(x, t)}{\partial x^2} - k_{\text{in}} c(x_{\text{in}}, t) \delta(x - x_{\text{in}}) + k_{\text{in}} c(x_{\text{in}}, t) \delta(x - x_{\text{out}}) \quad (8)$$

with the boundary conditions

$$\begin{aligned} Dc'_s(x=0) &= \left. \frac{dc_s}{dx} \right|_{x=0} = -k_{\text{CRAC}}, \\ Dc'_s(x=L) &= \left. \frac{dc_s}{dx} \right|_{x=L} = +k_{\text{PMCA}}c_s(x=L). \end{aligned} \quad (9)$$

$k_{\text{CRAC}}$  and  $k_{\text{PMCA}}$  are the strengths of the CRAC channel and PMCA pumps, respectively, and  $k_{\text{in}}$  is the strength of the mitochondrial uptake (determining also the release at the other end of the mitochondrion  $k_{\text{out}} = k_{\text{in}}c_s(x = x_{\text{in}})$ ).

### 3.1. Stationary $\text{Ca}^{2+}$ concentration profile

We are interested in the stationary solution  $c_s(x) = \lim_{t \rightarrow \infty} c(x, t)$  that is reached quickly due to fast  $\text{Ca}^{2+}$  diffusion. For this  $c_s''(x) = 0$  holds for  $x \neq x_{\text{in}}, x_{\text{out}}$ , implying that the function  $c_s(x)$  is piecewise linear (as depicted in figure 5) and of course continuous. At the points  $x = x_{\text{in}}$  and  $x_{\text{out}}$  the second derivative of  $c_s(x)$  has a delta-function part

$$Dc_s''(x) = +k_{\text{in}}c_s(x_{\text{in}})\delta(x - x_{\text{in}}) - k_{\text{in}}c_s(x_{\text{in}})\delta(x - x_{\text{out}}), \quad (10)$$

i.e. the first derivative jumps by

$$\Delta c'_s(x_{\text{in}, \text{out}}) = \lim_{\epsilon \rightarrow 0} \int_{x_{\text{in}, \text{out}} - \epsilon}^{x_{\text{in}, \text{out}} + \epsilon} dx c_s''(x) = \begin{cases} c_s(x_{\text{in}}) k_{\text{in}}/D & \text{for } x = x_{\text{in}}, \\ -c_s(x_{\text{in}}) k_{\text{in}}/D & \text{for } x = x_{\text{out}}. \end{cases} \quad (11)$$

As in figure 5 we denote  $c_0 = c_s(x = 0)$ ,  $c_1 = c_s(x = x_{\text{in}})$ ,  $c_2 = c_s(x = x_{\text{out}})$  and  $c_3 = c_s(x = L)$ . Moreover, we define  $l = x_{\text{out}} - x_{\text{in}}$ , the length of the mitochondrion, and the slopes  $\Delta_0 = (c_0 - c_1)/x_{\text{in}}$ ,  $\Delta_1 = (c_2 - c_1)/l$  and  $\Delta_2 = (c_2 - c_3)/(L - x_{\text{out}})$ , implying

$$\begin{aligned} c_1 &= c_0 - \Delta_0 x_{\text{in}}, \\ c_2 &= c_1 + \Delta_1 l, \\ c_3 &= c_2 - \Delta_2 (L - x_{\text{out}}). \end{aligned} \quad (12)$$

Additionally, from the boundary conditions (9)

$$\begin{aligned} \Delta_0 &= k_{\text{CRAC}}/D, \\ \Delta_2 &= k_{\text{PMCA}}c_3/D \end{aligned} \quad (13)$$

and from the jump conditions (11)

$$\begin{aligned} D\Delta_0 + D\Delta_1 &= c_1 k_{\text{in}}, \\ D\Delta_1 + D\Delta_2 &= c_1 k_{\text{in}}, \end{aligned} \quad (14)$$

we immediately obtain  $\Delta_2 = \Delta_0$  which is already indicated in figure 5. A bit of algebra leads to the solution

$$\begin{aligned} c_3 &= k_{\text{CRAC}}/k_{\text{PMCA}}, \\ c_2 &= k_{\text{CRAC}}/k_{\text{PMCA}} + k_{\text{CRAC}}(L - l - x_{\text{in}})/D, \\ c_1 &= c_2 (1 - (k_{\text{in}} - k_{\text{CRAC}})l/D)^{-1}, \\ c_0 &= \frac{k_{\text{CRAC}}/D}{1 + k_{\text{in}}l/D} (L + D/k_{\text{PMCA}} + x_{\text{in}}k_{\text{in}}l/D) \end{aligned} \quad (15)$$

that we will discuss below.

### 3.2. Parameter choice

To estimate a physiologically relevant parameter range, one first has to consider that the model is 1D, which means that physiologically relevant concentrations and reaction rates have to be adopted: concentrations in 1D are measured in the number of  $\text{Ca}^{2+}$  ions per micron, which is the inverse mean distance between  $\text{Ca}^{2+}$  ions. In three space dimensions,  $\text{Ca}^{2+}$  concentrations are measured in nM, i.e. in the number of  $\text{Ca}^{2+}$  ions per volume. The third root of this 3D concentration yields the inverse mean distance of  $\text{Ca}^{2+}$  ions in 3D, too. For instance, a  $\text{Ca}^{2+}$  concentration of 100 nM means 60  $\text{Ca}^{2+}$  ions per cubic micron, corresponding to an average distance of 1/4 micron between  $\text{Ca}^{2+}$  ions. Thus 100 nM corresponds in our model to a concentration to  $4 \mu\text{m}^{-1}$  (note that increasing the concentration in 1D increases the concentration in 3D by a factor of 8). Thus, we can translate  $\text{Ca}^{2+}$  concentrations in 1D ( $c_{1\text{D}}$ ) to  $\text{Ca}^{2+}$  concentrations in 3D ( $c_{3\text{D}}$ ) via the formula

$$c_{3\text{D}} \text{ (nM)} = 1.66(c_{1\text{D}} \mu\text{m})^3. \quad (16)$$

Moreover, inverse  $\text{Ca}^{2+}$  concentrations, as used for a measure of  $\text{Ca}^{2+}$  pumps, are related via  $c_{3\text{D}}^{-1} \text{ [(nM}^{-1})] = 0.6(c_{1\text{D}}^{-1} \mu\text{m}^{-1})^3$ . We assume that at  $x = L$  (the point with the largest distance from the IS) the  $\text{Ca}^{2+}$  concentration is ‘normal’, i.e.  $c_3 = c_{\text{rest}} = 4 \mu\text{m}^{-1}$ . A completely open single CRAC channel releases about  $10^4$   $\text{Ca}^{2+}$  ions per second [34], which means that in 3D

**Table 2.** Parameters of the 1D model.

	1D model	3D equivalent
$c_{\text{rest}}$	$4 \mu\text{m}^{-1}$	$0.1 \mu\text{M}$
$k_{\text{CRAC}}$	$100 \text{s}^{-1}$	$5 \times 10^6 \text{s}^{-1}$
$k_{\text{PMCA}}$	$25 \mu\text{m s}^{-1}$	$3.84 \times 10^5 \mu\text{M}^{-1} \text{s}^{-1}$
$k_{\text{in}}$	$25 \mu\text{m s}^{-1}$	$3.84 \times 10^5 \mu\text{M}^{-1} \text{s}^{-1}$
$L$	$10 \mu\text{m}$	
$l = x_{\text{out}} - x_{\text{in}}$	$1 \mu\text{m}$	
$x_{\text{in}}$	$0.1\text{--}5 \mu\text{m}$	

the CRAC rate is  $k_{\text{CRAC},3\text{D}} = 10^4 \text{s}^{-1}$  for a single channel. An assumed cluster of 50 channels corresponds in 1D to  $k_{\text{CRAC},1\text{D}} \approx 100 \text{s}^{-1}$ . Since  $c_3 = k_{\text{CRAC}}/k_{\text{PMCA}}$  and  $c_3$  and  $k$  are now fixed, we have for the PMCA rate  $k_{\text{PMCA}} = 25 \mu\text{m s}^{-1}$ . In the following, we consider the mitochondria rate  $k_{\text{in}}$  in relation to  $k_{\text{PMCA}}$ . The  $\text{Ca}^{2+}$  diffusion constant is set to  $D = 100 \mu\text{m}^2 \text{s}^{-1}$ , the cell size is  $L = 10 \mu\text{m}$  and the mitochondria length is  $l = 1 \mu\text{m}$  (results for  $l = 2$  and  $3 \mu\text{m}$ , see supplementary figures S1 and S2, available from [stacks.iop.org/NJP/15/055022/mmedia](http://stacks.iop.org/NJP/15/055022/mmedia)). The parameters are summarized in table 2.

### 3.3. Results

From equation (15), one observes immediately that independent of the choice of parameter values the  $\text{Ca}^{2+}$  concentration at the IS (close to  $x = 0$ ) increases with increasing distance between the mitochondria and the CRAC channels (i.e. increasing  $x_{\text{in}}$ ) and that the  $\text{Ca}^{2+}$  concentration in the center of the cell (i.e.  $c_2$  or the average  $(c_2 + c_3)/2$ ) decreases with increasing  $x_{\text{in}}$ . Thus the model predicts that mitochondria relocation toward the IS is sufficient to increase the global  $\text{Ca}^{2+}$  concentration when CRAC channels are active. Concomitantly, the  $\text{Ca}^{2+}$  concentration at the IS is reduced when mitochondria are close to the IS. Using the parameter defined above, we have calculated  $c_s(x)$  using equation (15). In figures 6(a) and (b) the  $\text{Ca}^{2+}$  concentration as a function of  $x$  is shown for different positions  $x_{\text{in}}$  of the mitochondria and different mitochondria rates  $k_{\text{in}}$ . As expected, the  $\text{Ca}^{2+}$  concentration at the IS decreases with decreasing distance of the mitochondria, whereas the  $\text{Ca}^{2+}$  concentration in the bulk increases with decreasing distance. The effect is most pronounced for high mitochondria rates, where also the  $\text{Ca}^{2+}$  concentration at the IS is, as expected, lowest. In figures 6(c) and (d) we compare the  $\text{Ca}^{2+}$  concentration at the IS,  $c_{\text{IS}} = c_0$  with the average global  $\text{Ca}^{2+}$  concentration,  $c_{\text{global}}$  defined as

$$\begin{aligned}
 c_{\text{global}} &= L^{-1} \int_0^L dx c_s(x) \\
 &= L^{-1} [x_{\text{in}}(c_0 + c_1)/2 + l(c_1 + c_2)/2 + (L - l - x_{\text{in}})(c_2 + c_3)/2]. \quad (17)
 \end{aligned}$$

The data are translated to 3D  $\text{Ca}^{2+}$  concentrations with the formula (16). In addition to the general trend that the global and IS  $\text{Ca}^{2+}$  concentrations follow opposite trends when varying the distance  $x_{\text{in}}$ , one can see that for large mitochondria rates the global  $\text{Ca}^{2+}$  concentration can even be higher than the  $\text{Ca}^{2+}$  concentration at the IS when the mitochondria are close to the IS. Here the increase of the global  $\text{Ca}^{2+}$  concentration when moving the mitochondria from

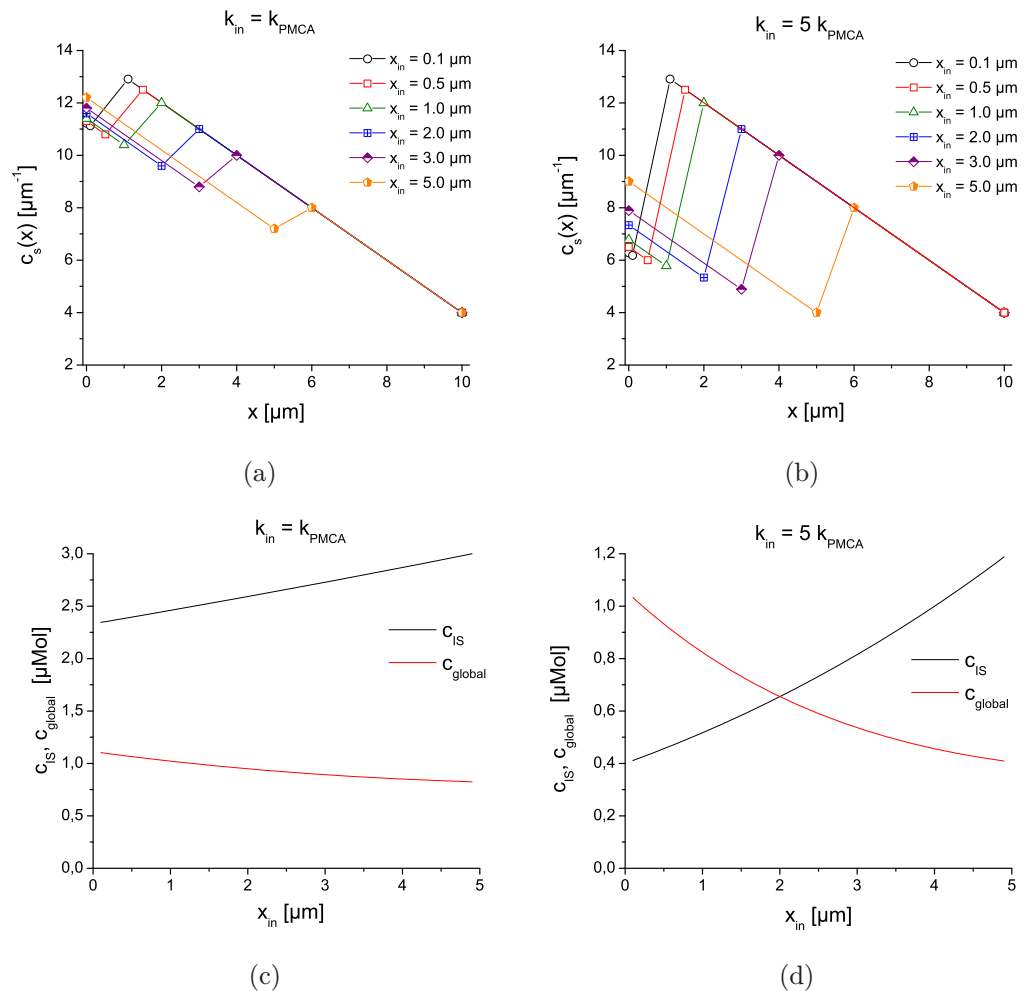


**Figure 6.** (a), (b) Stationary  $\text{Ca}^{2+}$  concentration  $c_s(x)$  as a function of  $x$  for different positions  $x_{in}$  of the mitochondria and different mitochondria rates  $k_{in}$ . (c), (d) Comparison of the stationary  $\text{Ca}^{2+}$  concentration at the IS,  $c_{IS} = c_0$  and the average global  $\text{Ca}^{2+}$  concentration  $c_{global}$  calculated with formula (17) as a function of the distance  $x_{in}$  between IS and mitochondria for different mitochondria rates  $k_{in}$ . The 1D  $\text{Ca}^{2+}$  concentration obtained by the model are translated into the corresponding 3D  $\text{Ca}^{2+}$  concentration measured in  $\mu\text{M}$  using equation (16).

the center of the cell to the IS is about 50%. One obtains qualitatively the same results if one considers some more complex variants of our model, for example by including  $\text{Ca}^{2+}$  diffusion inside the mitochondria or by assuming an additional PMCA pump at the cell's front end (see supplementary figures S3 and S4, available from [stacks.iop.org/NJP/15/055022/mmedia](http://stacks.iop.org/NJP/15/055022/mmedia)).

One might expect that moving a strong sink closer to the main  $\text{Ca}^{2+}$  source will decrease the  $\text{Ca}^{2+}$  concentration here and that the release of this absorbed  $\text{Ca}^{2+}$  at a distant site will increase the  $\text{Ca}^{2+}$  concentration there. But that the *total* amount of  $\text{Ca}^{2+}$  present in the cell will be substantially *increased* already by this simple redistribution without any further mechanisms involved appears to be a rather non-trivial prediction of this simple model.

## 4. $\text{Ca}^{2+}$ signaling during T-cell activation and polarization

### 4.1. Microdomains and global $\text{Ca}^{2+}$ during T-cell polarization

After the formation of an immunological synapse, the polarization of T-cells, the rearrangement of cell organelles and  $\text{Ca}^{2+}$  channels and pumps, starts. This polarization is essential for the calcium-dependent activation of T-cells that should finally end in destroying or killing the abnormal/antigen-presenting cell. For full activation, a sustained, robust and high  $\text{Ca}^{2+}$  signal of several minutes up to hours is needed. There is strong evidence that mitochondria, which act as  $\text{Ca}^{2+}$  buffer and distributors, are very important for full T-cell activation. It was shown that inhibition of mitochondrial calcium uptake diminished the cytosolic  $\text{Ca}^{2+}$  [35] and that mitochondria actively translocate to the IS [14, 15], where they are localized close to CRAC channels. There, mitochondria lower the  $\text{Ca}^{2+}$  microdomain right at the IS and thus prevent the calcium-dependent inactivation of the CRAC channels. Besides, a redistribution and accumulation of PMCA pumps beneath mitochondria right after IS formation is observed [15], which decreases the calcium export locally and in the end leads to higher global  $\text{Ca}^{2+}$  signals. Hence, one could expect the distance between the opened CRAC channel and the mitochondria to be the dominant physical determinant of spatial  $\text{Ca}^{2+}$  signals. We therefore want to answer the questions whether the distance between IS and mitochondria influence the global  $\text{Ca}^{2+}$  concentration and the local  $\text{Ca}^{2+}$  microdomain at the IS simultaneously and whether the redistribution of PMCA pumps is a necessary effect in T-cell activation. Furthermore, we want to study the role of active SERCA pumps, which under physiological conditions refill the ER, and the influence of ER position on the resulting  $\text{Ca}^{2+}$  signals.

### 4.2. The three-dimensional full cell reaction–diffusion model

As mentioned above, the up-regulation of the cytosolic  $\text{Ca}^{2+}$  concentration during T-cell activation is a result of a complex interplay between several cell compartments (cytosol, mitochondria, ER, etc) and different  $\text{Ca}^{2+}$  channels and pumps that transfer  $\text{Ca}^{2+}$  from one compartment to the other. To understand the effect of mitochondria relocation within the cytosol and the PMCA pump accumulation on the spatial distribution on  $\text{Ca}^{2+}$ , for example, we developed a 3D full cell model for the  $\text{Ca}^{2+}$  dynamics during T-cell activation. We assume an ideal spherical T-cell with radius  $r_{\text{cell}} = 4 \mu\text{m}$ . 2D microscopy images of T-cells deliver the estimate that the cell nucleus covers about half and mitochondria about 10% of the cell area. Modeling a spherical nucleus and tori- or rod-like mitochondria, this estimate leads to a radius  $r_{\text{nuc}} = r_{\text{cell}}/2$  and four to ten mitochondria with a length of  $3.5 \mu\text{m}$  and a diameter of  $d_{\text{M}} = 300 \text{ nm}$ .

In our simulations, eight mitochondria at a distance of  $x_{\text{Mito}}$  to the IS can take up  $\text{Ca}^{2+}$  at their upper tip pointing toward the IS (yellow surface, see figure 7) and release it at the opposite end. Within the mitochondria,  $\text{Ca}^{2+}$  diffuses with diffusion constant  $D_{\text{M}}$ . At the IS, we assume an accumulation of CRAC channels into a cluster of radius  $r_{\text{CRAC}} = 0.1 \mu\text{m}$ . At a distance of  $0.3 \mu\text{m}$  to this CRAC cluster, a spherical segment of 100 nm width represents an agglomerate of PMCA pumps. In our Base Case scenario this spherical segment contains 50% of all pumps, whereas the other 50% are homogeneously distributed over the whole cell PM. Inside the cytosol, calcium is buffered by a mobile  $\text{Ca}^{2+}$  buffer  $b$  that freely diffuses with constant  $D_b$ . The total amount of buffer  $[b]_{\text{T}} = [b] + [bc]$  is initially uniform in the cytosol for which we assumed that the binding of calcium does not change the diffusion properties of the

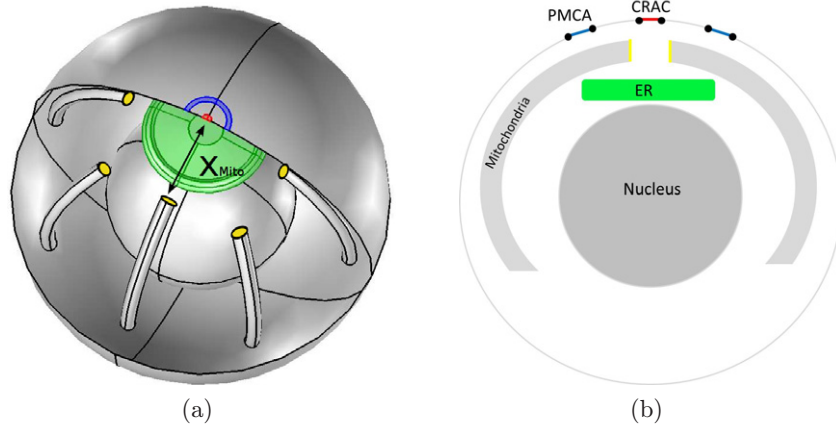


**Figure 7.** (a) 3D model geometry for studying the effect of mitochondria relocation on  $\text{Ca}^{2+}$  influx at the IS in T-cells. The outer shell indicates the cell membrane, the inner sphere the nucleus and the circular region at the top, the IS. Around the IS the CRAC channels (red) and the PMCA pumps (blue) agglomerate. The green compartment indicates the ER, the rod-like objects with yellow tips indicate the mitochondria and the black arrow indicates the distance  $x_{\text{Mito}}$  between mitochondria and IS. (b) 2D ( $x$ - $z$  plane) profile of the model geometry.

buffer. In addition to the cytosol and mitochondria, the ER (green volume, see figure 7) is the third compartment that completes our simulation geometry. The naturally very thin ER network is modeled as a massive domain and therefore we assume open flux conditions for the cytosolic calcium  $c_{\text{cyt}}$  at cytosol–ER boundaries, which means that cytosolic calcium freely diffuses through the ER domain. Our model geometry that consists of the complete cell subtracted by the nucleus is the sum of three disjunct compartments: the cytosol, the ER and eight mitochondria. Within these three different compartments the  $\text{Ca}^{2+}$  dynamics are described by the following reaction–diffusion equations:

$$\text{Cytosol: } \frac{\partial c_{\text{cyt}}}{\partial t} = D_{\text{cyt}} \nabla^2 c_{\text{cyt}} - k_1 c_{\text{cyt}} b + k_2 bc, \quad (18)$$

$$\frac{\partial b}{\partial t} = D_b \nabla^2 b - k_1 c_{\text{cyt}} b + k_2 bc, \quad (19)$$

$$\frac{\partial bc}{\partial t} = D_{bc} \nabla^2 bc + k_1 c_{\text{cyt}} b - k_2 bc. \quad (20)$$

$$\text{Mitochondria: } \frac{\partial c_{\text{M}}}{\partial t} = D_{\text{M}} \nabla^2 c_{\text{M}}. \quad (21)$$

$$\text{ER: } \frac{\partial c_{\text{ER}}}{\partial t} = D_{\text{ER}} \nabla^2 c_{\text{ER}}. \quad (22)$$

The calcium transfer between these 3D compartments and the  $\text{Ca}^{2+}$  in/outflow across the cell plasma membrane  $J_{\text{M}}$ ,  $J_{\text{ER}}$  and  $J_{\text{PM}}$  are described as flux/boundary conditions on particular 2D surfaces. The  $\text{Ca}^{2+}$  exchange through the cell membrane  $J_{\text{PM}}$  can be decomposed into two

contributions,  $J_{\text{PM}} = J_{\text{CRAC}} - J_{\text{PMCA}}$ , the influx from the CRAC channels and the  $\text{Ca}^{2+}$  pumped out of the cytosol by the PMCA pumps.  $J_{\text{CRAC}}$  is only defined on the CRAC cluster surface (red area in figure 7). The cluster influx is coupled to the  $\text{Ca}^{2+}$  concentration within the ER ( $c_{\text{ER}}$ ) and at the average  $\text{Ca}^{2+}$  concentration ( $c_{\text{cyt}}^{(\text{micro})}$ ) in the microdomain around the cluster in the following way:

$$J_{\text{CRAC}} = k_{\text{CRAC}} f(c_{\text{ER}}) g_{c_{1/2}, \Delta c}(c_{\text{cyt}}^{(\text{micro})}), \quad (23)$$

where  $f(x)$  and  $g(x)$  are both smooth sigmoidal-shaped functions modeling the CRAC activation by emptied ER and CRAC inhibition by an enhanced  $\text{Ca}^{2+}$  concentration in the microdomain, respectively. We assume  $f(x) = 0$  for a full store  $x > 10 \mu\text{mol}$  and  $f(x) = 1$  for an empty store ( $x = 0$ ).  $g_{c_{1/2}, \Delta c}(x)$  varies smoothly from  $g(x) = 1$  for  $x \leq c_{1/2} - \Delta c$  to  $g(x) = 0$  for  $x \geq c_{1/2} + \Delta c$ .

The  $\text{Ca}^{2+}$  removal from the cytosol through the plasma membrane by PMCA pumps is given by

$$J_{\text{PMCA,PM}} = k_{\text{PMCA,PM}} \frac{c_{\text{cyt}}}{k_p + c_{\text{cyt}}}, \quad (24)$$

where the parameter  $k_p$  represents the  $\text{Ca}^{2+}$  concentration at which the pumps work at half maximal efficiency  $k_{\text{PMCA,PM}}$ , and

$$J_{\text{PMCA,IS}} = k_{\text{PMCA,IS}} \frac{c_{\text{cyt}}}{k_p + c_{\text{cyt}}}. \quad (25)$$

This form reflects the fact that the activity of the PMCA pump increases with  $\text{Ca}^{2+}$  concentration in the cytosol [36–38].  $J_{\text{PMCA,IS}}$  describes the flux through the PMCA pumps, which are accumulated in the spherical segment around the IS, and  $J_{\text{PMCA,PM}}$  describes the flux through the residual plasma membrane.

The  $\text{Ca}^{2+}$  exchange of the ER is restricted to the ER surface (green area, see figure 7) and the flux  $J_{\text{ER}}$  can also be decomposed into two contributions,  $J_{\text{ER}} = J_{\text{IP}_3} - J_{\text{SERCA}}$ , the  $\text{Ca}^{2+}$  release by the  $\text{IP}_3$  receptors and the  $\text{Ca}^{2+}$  pumped back into the ER by the SERCAs. In our simulations we assume fully activated  $\text{IP}_3$  receptor channels during the specified time period  $t_{\text{IP}_3}$ . For time  $t > t_{\text{IP}_3}$  the flux  $J_{\text{IP}_3}$  is equal to zero; otherwise it is given by a constant release rate multiplied with the ER  $\text{Ca}^{2+}$  concentration:

$$J_{\text{IP}_3} = k_{\text{IP}_3} c_{\text{ER}}. \quad (26)$$

For a modified flux including the calcium-induced inhibition of the  $\text{IP}_3$  receptor the results do not change significantly.

The  $\text{Ca}^{2+}$  back-flux into the ER caused by the SERCA pumps is

$$J_{\text{SERCA}} = k_{\text{SERCA}} c_{\text{cyt}} j(c_{\text{cyt}}), \quad (27)$$

where  $j(c_{\text{cyt}})$  is a smoothed sigmoidal function that is zero for a cytosolic concentration of 0 nM and reaches its maximum value of one for concentrations around 400 nM. The  $\text{Ca}^{2+}$  uptake, release and redistribution by mitochondria is given by the flux

$$J_{\text{M}} = -k_{\text{M}_{\text{in}}} c_{\text{cyt}} + k_{\text{M}_{\text{out}}} c_{\text{M}}, \quad (28)$$

where  $k_{\text{M}_{\text{in}}} c_{\text{cyt}}$  describes the  $\text{Ca}^{2+}$  uptake at the tube ends pointing toward the IS (see figure 7, yellow surfaces). The release of mitochondrial  $\text{Ca}^{2+}$  is described by the boundary condition



$k_{M,out} c_M$  at the opposite tube ends. The mitochondrial  $Ca^{2+}$  uptake in our model depends on the cytosolic concentration  $c_{cyt}$ , whereas the  $Ca^{2+}$  release is a function of the buffered  $Ca^{2+}$  inside the mitochondria,  $c_M$ . This simplified description of mitochondrial  $Ca^{2+}$  uptake and release, only possible at the circular mitochondria ends, saves computational time and leads qualitatively to the same results as a more realistic mitochondria modeling with  $Ca^{2+}$  uptake and release that is defined on the complete mitochondria/cytosol interface.

With our model we want to study two different scenarios, an ‘experiments-like’ case and a more physiological one. The first addresses most experiments concerning  $Ca^{2+}$  signaling in T-cells, which make use of tapsigargin. Tapsigargin is a drug that blocks the SERCA pumps, thus leading to a completely depleted ER and fully activated CRAC channels. In this case we just neglect the ER compartment with its  $IP_3$  channels and SERCA pumps and assume a fully activated CRAC channel that is only inhibited by the formation of a microdomain around the channel. As a consequence, equation (22) and the boundary condition defining the flux  $J_{ER}$  are omitted, and equation (23) changes to  $J_{CRAC} = k_{CRAC} g(c_{cyt}^{(micro)})$ .

Considering the full set of equations and boundary conditions defined above allows us to study a more physiological scenario that is very hard or nearly impossible to investigate in experiments. In this case we analyze  $Ca^{2+}$  signaling with active SERCA pumps, a fully loaded ER at time  $t = 0$  and a predetermined  $IP_3$  stimulus of duration  $t_{IP_3}$ . As long as this stimulus is present, the  $IP_3$  channels release  $Ca^{2+}$  out of the ER, thereby activating the CRAC channels and leading to a  $Ca^{2+}$  influx into the cell. The channel activation causes a rise of the cytosolic  $Ca^{2+}$  concentration and a refilling of the ER by the SERCA pumps, thus leading to a partial inhibition of the CRAC channels.

To solve our reaction–diffusion equations, we use the package ‘transport of diluted species’ of the finite elements method software ‘Comsol’ (<http://www.comsol.com/>).

### 4.3. Parameter values

As the diffusion coefficient of free cytosolic and mitochondrial  $Ca^{2+}$ , we use the value measured by Allbritton *et al* [39],  $D_{cyt} = D_M = 220 \text{ } (\mu\text{m}^2 \text{ s}^{-1})$ . Because of the internal organelle structure, the diffusion coefficient in mitochondria should be smaller than for free cytosolic diffusion. But a variation of the coefficient  $D_M$  does not change the results for the stationary  $Ca^{2+}$  profiles (data not shown). The diffusion coefficient in the ER is about a factor of 2–5 smaller than in the cytosol because of the tubular ER structure [40, 41]. Mobile  $Ca^{2+}$  buffers normally diffuse with a diffusion coefficient of one-tenth to one-half that of free  $Ca^{2+}$  [42]. The reaction rates for  $Ca^{2+}$  binding and unbinding,  $k_1$  and  $k_2$ , and the buffer resting concentration of  $c_b(t = 0)$  are in good agreement with commonly used modeling parameters [5]. The channel cluster with an area of  $A_{CRAC} = 3.0 \times 10^{-14} \text{ m}^2$  consists of about 40–60 active channels; each one, if fully activated, pumps  $10^4$   $Ca^{2+}$  ions per second into the cell [43]. This leads to a CRAC channel influx parameter of about  $k_{CRAC} \approx 3 \times 10^{-5} \text{ mol}/(\text{m}^2 \text{ s})$ . Note that in our Base Case scenario 50% of all PMCA pumps are located in the spherical segment at the IS (see figure 7). The surface ratio of the plasma membrane and the spherical segment  $A_{PM}/A_{segment} = 720$  leads to the relation  $k_{PMCA,PM} = k_{PMCA,IS}/720$  for the two maximum current sizes.

The maximum PMCA clearance rate in T-cells is in the range of 50–200  $\text{nM s}^{-1}$  [38], which if multiplied with our simulated cell volume ( $2.7 \times 10^{-13} \text{ dm}^3$ ) would lead to a maximum PMCA clearance of  $0.5 \times 10^{-19} \text{ mol s}^{-1}$ . In our Base Case scenario the maximum value of the PMCA current is  $I_{PMCA}^{\max} = 2A_{PM}k_{PMCA}^{\max} = 1.12 \times 10^{-18} \text{ mol s}^{-1}$ , which is in good agreement with other

**Table 3.** Parameters and initial values used for the Base Case scenario in our 3D cell model.

Parameter	Value (unit)	Parameter	Value (unit)
$D_{\text{cyt}}$	220 ( $\mu\text{m}^2 \text{s}^{-1}$ )	$k_1$	100 ( $\text{m}^3 (\text{mol s})^{-1}$ )
$D_{\text{M}}$	220 ( $\mu\text{m}^2 \text{s}^{-1}$ )	$k_2$	0.3 ( $\text{s}^{-1}$ )
$D_b$	20 ( $\mu\text{m}^2 \text{s}^{-1}$ )	$k_{\text{M}_{\text{in}}}$	$4 \times 10^{-2}$ ( $\text{m s}^{-1}$ )
$D_{bc}$	20 ( $\mu\text{m}^2 \text{s}^{-1}$ )	$k_{\text{M}_{\text{out}}}$	$2 \times 10^{-3}$ ( $\text{m s}^{-1}$ )
$D_{\text{ER}}$	100 ( $\mu\text{m}^2 \text{s}^{-1}$ )	$k_{\text{SERCA}}$	$10^{-5}$ ( $\text{m s}^{-1}$ )
$c_{\text{cyt}}(t=0)$	100 (nmol)	$k_{\text{IP}_3}$	$10^{-8}$ ( $\text{m s}^{-1}$ )
$c_{\text{M}}(t=0)$	100 (nmol)	$k_{\text{CRAC}}$	$4 \times 10^{-5}$ ( $\text{mol} (\text{m}^2 \text{s})^{-1}$ )
$c_{\text{ER}}(t=0)$	10 ( $\mu\text{mol}$ )	$k_{\text{PMCA}}$	$2.8 \times 10^{-9}$ ( $\text{mol} (\text{m}^2 \text{s}^{-1})$ )
$c_b(t=0)$	10 ( $\mu\text{mol}$ )	$k_p$	0.25 ( $\mu\text{mol}$ )
$c_{bc}(t=0)$	0.5 ( $\mu\text{mol}$ )	$c_{1/2}$	7.5 ( $\mu\text{mol}$ )
$A_{\text{CRAC}}$	$3.04 \times 10^{-14} \text{m}^2$	$\Delta c$	6.5 ( $\mu\text{mol}$ )
$A_{\text{PM}}$	$2.0 \times 10^{-10} \text{m}^2$	$A_{\text{M}}$	$5.08 \times 10^{-13} \text{m}^2$

theoretical work [44, 45]. The maximum calcium clearance by mitochondria can be estimated as  $I_{\text{M}}^{\text{max}} = A_{\text{M}} k_{\text{M}}^{\text{max}} c \approx 1 \times 10^{-18} \text{mol s}^{-1}$ , where  $c = 20\text{--}50 \text{nM}$  is the  $\text{Ca}^{2+}$  concentration that is averaged over the  $\text{Ca}^{2+}$  uptaking mitochondria surfaces (yellow area, see figure 7). With the resulting ratio  $I_{\text{PMCA}}^{\text{max}}/I_{\text{M}}^{\text{max}} \approx 1$  our parameter choice is in very good agreement with the known experimental result that in T-cells calcium clearance by mitochondria and calcium clearance by PMCA pumps are within the same range of magnitude [15, 38, 46, 47]. The robustness of our results with respect to a variation of the ratio  $I_{\text{PMCA}}^{\text{max}}/I_{\text{M}}^{\text{max}}$  is discussed in supplementary figure S5 (available from [stacks.iop.org/NJP/15/055022/mmedia](http://stacks.iop.org/NJP/15/055022/mmedia)). There we also show qualitatively the same results for a different ansatz for the  $\text{Ca}^{2+}$  uptake and release by mitochondria,  $J_{\text{M}} = k_{\text{M}_{\text{in}}} \frac{c_{\text{cyt}}^2}{k_{\text{M}_1}^2 + c_{\text{cyt}}^2} - k_{\text{M}_{\text{out}}} \frac{c_{\text{M}}}{k_{\text{M}_2} + c_{\text{M}}}$ , and again obtain the robustness of these results with respect to a variation of the ratio  $I_{\text{PMCA}}^{\text{max}}/I_{\text{M}}^{\text{max}}$ .

The initial values, reaction/diffusion parameters and other parameter values we used as a Base Case scenario are summarized in table 3.

#### 4.4. Results

**4.4.1. Disabled sarcoplasmic/endoplasmic reticulum calcium ATPase (SERCA) pumps and the influence of mitochondria and plasma membrane  $\text{Ca}^{2+}$  ATPase pump location.** First, we present results that are obtained with our model assuming active CRAC channels and disabled SERCA pumps (experimentally realized by the SERCA inhibitor thapsigargin), neglecting the ER domain. In figure 8 snapshots of the resulting spatio-temporal evolution of the  $\text{Ca}^{2+}$  concentration are shown for mitochondria close to the CRAC channels ( $x_{\text{in}} = 0.1 \mu\text{m}$ ). Further snapshots are shown in supplementary figures S6 and S7 (available from [stacks.iop.org/NJP/15/055022/mmedia](http://stacks.iop.org/NJP/15/055022/mmedia)). After a few seconds the  $\text{Ca}^{2+}$  distribution reaches a stationary state that is now evaluated further.

The stationary local and global  $\text{Ca}^{2+}$  concentrations as functions of mitochondria position  $x_{\text{Mito}}$  for our Base Case scenario are shown in figure 9(a). The local or microdomain concentration is computed by averaging the cytosolic  $\text{Ca}^{2+}$  in a 100 nm sphere with origin in the middle of the CRAC cluster. Analogous to the 1D results, our 3D model predicts that

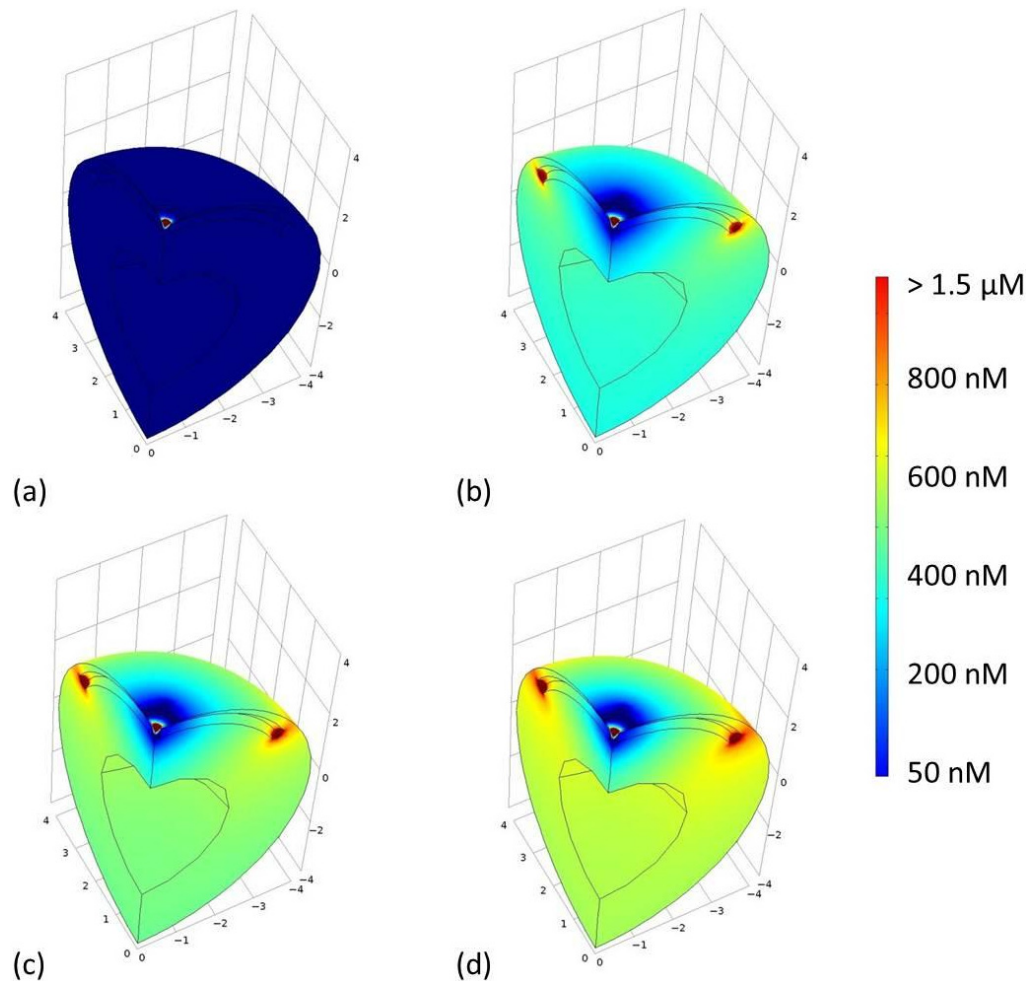


**Figure 8.** 3D snapshots of the spatio-temporal evolution of the cytosolic  $\text{Ca}^{2+}$  concentration  $c_{\text{cyt}}$ . Shown is a quarter of the cell geometry and the surface concentration of the visible geometry for a mitochondria position  $x_{\text{in}} = 0.1 \mu\text{m}$ . Parameters that are used for these calculations are discussed in section 4.3 and shown in table 3 in the main text. (a)  $t = 0$  s, (b)  $t = 5$  s, (c)  $t = 10$  s and (d)  $t = 20$  s.

mitochondria relocation or their relative position to the IS,  $x_{\text{Mito}}$ , controls  $\text{Ca}^{2+}$  microdomains as well as global  $\text{Ca}^{2+}$  signals when CRAC channels are active. By moving the mitochondria tip, which represents a sink, closer to the source of  $\text{Ca}^{2+}$  influx, the local  $\text{Ca}^{2+}$  microdomain is lowered as expected. Concomitantly the global  $\text{Ca}^{2+}$ , which is the average concentration over the whole cell, is increased if mitochondria are close to the IS.

The inset of figure 9(a) shows results for a case that is reminiscent of the geometrical arrangement in our 1D model (see section 3). In this scenario, 50% of PMCA pumps accumulate at the pole opposite the IS. This unphysiological model geometry also reveals that mitochondria position  $x_{\text{Mito}}$  controls  $\text{Ca}^{2+}$  signals; however, the dependence of  $\text{Ca}^{2+}$  on the mitochondria position is not as steep. In this case the pumps are located in a region of low  $\text{Ca}^{2+}$  concentration and are thus not that efficient. 3D snapshots of the spatio-temporal evolution of the global  $\text{Ca}^{2+}$

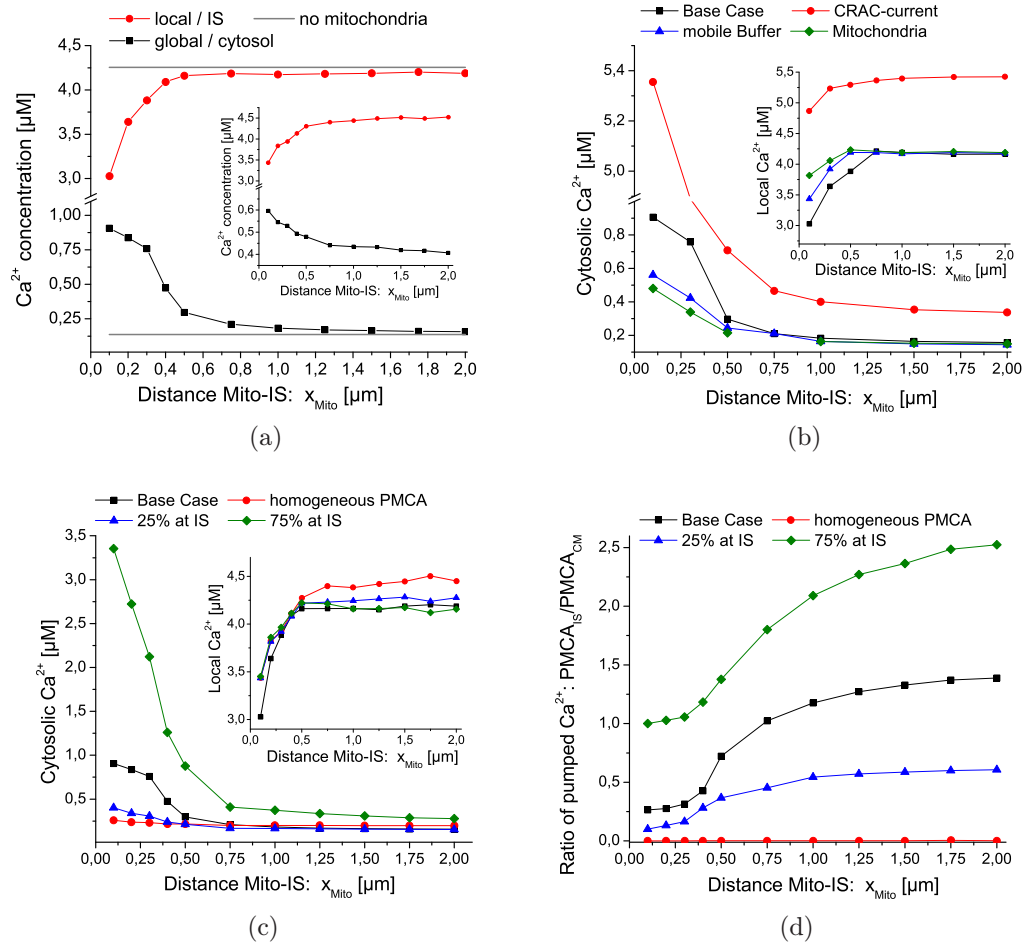


**Figure 9.** (a) Local (100 nm microdomain) and global (cytosol) stationary Ca<sup>2+</sup> signals as a function of the distance mitochondria–immunological synapse  $x_{\text{Mito}}$ . The horizontal constant gray lines indicate the Ca<sup>2+</sup> signals without mitochondria,  $k_{\text{Min}} = 0$ . Inset: the PMCA pump accumulation not around the IS but around the opposite cell pole. (b) Global and local Ca<sup>2+</sup> signals as a function of  $x_{\text{Mito}}$  for the Base Case scenario, more mobile Ca<sup>2+</sup> buffer (100 mM), stronger CRAC current ( $k_{\text{CRAC}} = 2 \times 10^{-4} (\text{mol} (\text{m}^2 \text{s})^{-1})$ ) and weaker mitochondrial Ca<sup>2+</sup> uptake/redistribution ( $k_{\text{Min}} = 4 \times 10^{-3} (\text{mol} (\text{m}^2 \text{s})^{-1})$ ,  $k_{\text{Mout}} = 2 \times 10^{-4} (\text{mol} (\text{m}^2 \text{s})^{-1})$ ). (c) Ca<sup>2+</sup> signals for different PMCA pump accumulations around the IS. (d) Ratio of Ca<sup>2+</sup> that is pumped out of the cell by the PMCA cluster around the IS and the homogeneously distributed pumps in the cell membrane.

signals that correspond to figure 9(a) are shown in supplementary figures S6 and S7 (available from [stacks.iop.org/NJP/15/055022/mmedia](http://stacks.iop.org/NJP/15/055022/mmedia)).

The strong dependence of Ca<sup>2+</sup> signals on the value of  $x_{\text{Mito}}$  is very robust under parameter changes, similar to what we found for the simplified 1D model described in the last section and in [15]. In figure 9(b) this robustness is demonstrated for stronger CRAC channel current, higher concentration of mobile buffers and enhanced mitochondrial Ca<sup>2+</sup> uptake and release. The same

holds for changing further parameters, for example for weaker or stronger PMCA pumps or for a different ansatz for the mitochondrial  $\text{Ca}^{2+}$  uptake and release (see supplementary figure S5 (available from [stacks.iop.org/NJP/15/055022/mmedia](http://stacks.iop.org/NJP/15/055022/mmedia))).

Although a lower microdomain  $\text{Ca}^{2+}$  concentration inflicted by close mitochondria reduces CRAC channel inhibition (see equation (23)) and thus might lead to higher  $\text{Ca}^{2+}$  influx, our model predicts an even more important role for the location of the PMCA pumps. We find that in addition to mitochondria relocation, the redistribution and accumulation of PMCA pumps near the IS are essential for high global  $\text{Ca}^{2+}$  signals and thereby for T-cell activation. The ratio of PMCA pumps located at the IS and the pumps in the remaining PM is the only parameter we found that reduces or even cancels the influence of mitochondria position on the observed stationary global  $\text{Ca}^{2+}$  signals. If one neglects the experimentally observed PMCA enrichment around the IS [15] and assumes a uniform pump distribution over the whole cell membrane, the global  $\text{Ca}^{2+}$  signals do not depend on the parameter  $x_{\text{Mito}}$  anymore (see figure 9(c)). A fatal consequence for T-cell activation is the fact that under these conditions no high global  $\text{Ca}^{2+}$  signals exist.

To understand this strong impact of PMCA pump distribution, we plotted the ratio of  $\text{Ca}^{2+}$  pumped out by PMCA pumps located around the IS,  $\text{PMCA}_{\text{IS}}$ , and by the pumps that are uniformly distributed in the PM,  $\text{PMCA}_{\text{CM}}$  (see figure 9(d)). Competition between the mitochondria and the PMCA pumps for the incoming  $\text{Ca}^{2+}$  takes place. For mitochondria close to the IS, they win this competition and the more PMCA pumps accumulated around the IS, the less  $\text{Ca}^{2+}$  pumped out of the cell, thereby increasing the global  $\text{Ca}^{2+}$  concentration. For mitochondria near the IS ( $x_{\text{Mito}} < 300$  nm), the amount of  $\text{Ca}^{2+}$  pumped out by the PMCA pumps located around the IS is small (about 20% for Base Case) compared to the amount of  $\text{Ca}^{2+}$  pumped out by the pumps which are distributed in the cell membrane. On the other hand, one can see that mitochondria position becomes increasingly important as more PMCA pumps are accumulated at the IS. For a uniform PMCA pump distribution, the ratio  $\text{PMCA}_{\text{IS}}/\text{PMCA}_{\text{CM}}$  is nearly zero, independent of the mitochondria position  $x_{\text{Mito}}$ , just because of the huge surface ratio  $A_{\text{CM}}/A_{\text{IS}} = 720$ .

**4.4.2. Active SERCA pumps and the influence of endoplasmic reticulum/SERCA location.** In the second part (see figure 10) we present the results of our model including the ER domain with active SERCA pumps,  $\text{IP}_3$  receptors and a CRAC channel current that senses the ER filling level. 3D snapshots of the spatio-temporal evolution of the  $\text{Ca}^{2+}$  signal are shown in supplementary figures S8 and S9 (available from [stacks.iop.org/NJP/15/055022/mmedia](http://stacks.iop.org/NJP/15/055022/mmedia)). The temporal evolution of the cytosolic/global  $\text{Ca}^{2+}$  signal for different mitochondria positions is shown in figure 10(a). Assuming a constant  $\text{IP}_3$  signal for the complete simulation time  $t_{\text{IP}_3} = 250$  s, the model predicts, analogous to the former case without ER depletion and refilling, a strong dependence of the global  $\text{Ca}^{2+}$  signal on the mitochondria position. We also find that in ‘stationary’ state the CRAC channel currents are stronger for mitochondria closer to the IS but a complete refilling of the ER accompanied by a CRAC channel inactivation is not observed. For a smaller time period of active  $\text{IP}_3$  receptors  $t_{\text{IP}_3} = 30$  s (see figure 10(b)), we find a partial CRAC channel inactivation caused by ER refilling. This channel inactivation and refilling of the ER is fastest for small values of  $x_{\text{Mito}}$  because of the higher global  $\text{Ca}^{2+}$  signal that was reached for times  $t < t_{\text{IP}_3}$ .

These results change dramatically (see figures 10(c) and (d)) if we change our geometry. Instead of a homogeneous SERCA pump distribution in the ER membrane we now assume

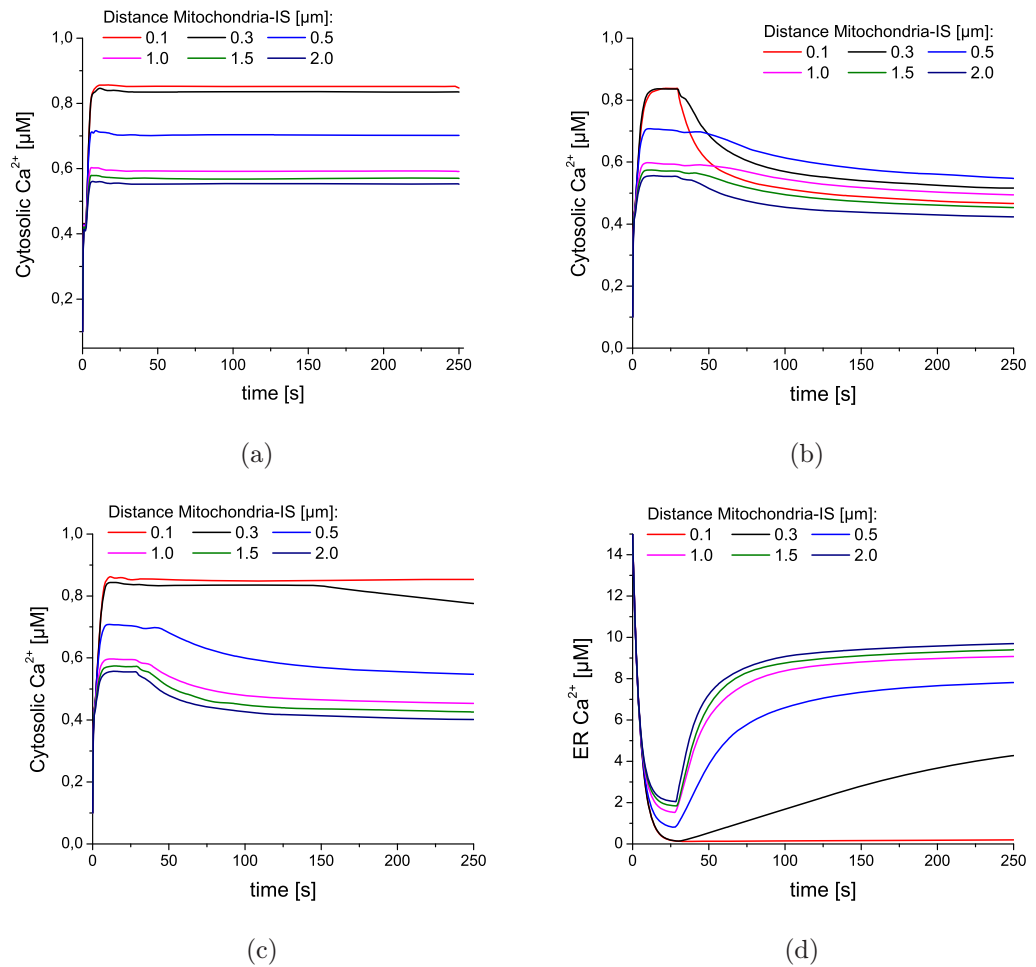


**Figure 10.** Ca<sup>2+</sup> in the cytosol and the ER for different durations of the IP<sub>3</sub> signals and under different SERCA pump distributions. We assume immobile mitochondria at a distance  $x_{\text{Mito}}$  to the IS. (a) Temporal evolution of global Ca<sup>2+</sup>. SERCA pumps are uniformly distributed and IP<sub>3</sub> is present during the whole simulation time,  $t_{\text{IP}_3} = 250$  s. (b) Temporal evolution of global Ca<sup>2+</sup> with uniformly distributed SERCAs and  $t_{\text{IP}_3} = 30$  s. (c) Temporal evolution of global Ca<sup>2+</sup>. SERCA pumps are accumulated near the IS and IP<sub>3</sub> is only present for the first 30 s. (d) ER Ca<sup>2+</sup> as function of time (accumulated SERCA pumps and  $t_{\text{IP}_3} = 30$  s).

that all SERCA pumps cluster in a circle of 350 nm diameter (see figure 6(a), circle in the middle of the ER domain) underneath the IS. Assuming a transient IP<sub>3</sub> signal we find, as for the case of non-clustering SERCAs, a refilling of the ER that leads to a partial inactivation of the CRAC channel current and consequently to a drop of the global Ca<sup>2+</sup> concentration. But in contrast to a uniform SERCA pump distribution, one finds that cells with mitochondria at short distance from the IS ( $x_{\text{Mito}} < 300$  nm) are able to maintain a high global Ca<sup>2+</sup> signal (see figure 10(c)), even in the absence of IP<sub>3</sub>, for times  $t > t_{\text{IP}_3}$ . This is possible because mitochondria win the competition for Ca<sup>2+</sup> ions against the PMCA and SERCA pumps, thereby reducing the store refilling (see figure 10(d)) and thus reducing the CRAC current inactivation.

Qualitatively, these results change neither by assuming a more sophisticated ER geometry nor by assuming a different ansatz for the  $\text{Ca}^{2+}$  back-flux into the ER caused by the SERCA pumps (see supplementary figure S10, available from [stacks.iop.org/NJP/15/055022/mmedia](http://stacks.iop.org/NJP/15/055022/mmedia)). Overall, our model predicts even for transient  $\text{IP}_3$  presence a sustained, robust and high  $\text{Ca}^{2+}$  signal that is needed for full T-cell activation if cell polarization managed to bring mitochondria close to the IS with a simultaneous SERCA pump accumulation in this region.

## 5. Discussion

The magnitude and duration of  $\text{Ca}^{2+}$  signals are very important and offer the possibility of inducing different immune responses such as tolerance, strong activation or apoptosis. For T-cell proliferation and activation, a high and robust  $\text{Ca}^{2+}$  signal for minutes up to hours is needed. To obtain such a high and robust signal, one has to postulate that  $\text{Ca}^{2+}$ -dependent CRAC channel inactivation has to be reduced. As a consequence, local  $\text{Ca}^{2+}$  microdomain concentration around the channel as well as the ER store refilling would have to be lowered. In this paper, we analyzed how the interplay of channels, pumps and organelle relocation leads to different  $\text{Ca}^{2+}$  microdomains and thereby to different global  $\text{Ca}^{2+}$  signals. The understanding of these complex mechanisms will help to elucidate physiological and pathophysiological T-cell activation.

Already in a highly simplified 1D model we could demonstrate the importance of mitochondria relocation toward the opened CRAC channels for the total cytosolic  $\text{Ca}^{2+}$  content of the T-cell. Our physiologically more realistic 3D model presented in this paper confirms this result that the relative position between mitochondria and the IS  $x_{\text{Mito}}$  indeed controls the stationary global  $\text{Ca}^{2+}$  signal and this result is very robust under parameter changes.

It should be emphasized that the model also demonstrates that a direct inhibition of a  $\text{Ca}^{2+}$ -dependent inactivation mechanism of CRAC channels is not necessary for sustained Ca influx: the decrease of  $\text{Ca}^{2+}$  concentration at the IS is a *consequence* of mitochondria relocation and  $\text{Ca}^{2+}$  uptake, not a premise for it. From a physical point of view it is also hard to imagine how  $\text{Ca}^{2+}$  uptake at 100–300 nM distance from the CRAC channels could prevent intruding  $\text{Ca}^{2+}$  from inactivating CRAC channels if  $\text{Ca}^{2+}$ -binding sites at the CRAC channel are involved.

Interestingly, the model predicts that for mitochondria relocation to have an effect on the global  $\text{Ca}^{2+}$  concentration, the PMCA pumps have to be distributed inhomogeneously over the PM. This effect is maximal for an accumulation of PMCA pumps around the IS, as actually observed experimentally [15]. In this case it is plausible that mitochondria relocation toward the IS has such a drastic effect on the global  $\text{Ca}^{2+}$  concentration: they prevent the PMCA pumps that are in the close vicinity of the opened CRAC channels extruding the intruded  $\text{Ca}^{2+}$  right away by absorbing it on the spot and redistributing it further inside the cytosol again. Surprisingly, PMCA accumulation at a position opposed to the IS is also sufficient to render the global  $\text{Ca}^{2+}$  concentration mitochondria position-dependent, which is reminiscent of what happens in the 1D model. Since in this case there is no competition between mitochondria and PMCA  $\text{Ca}^{2+}$  uptake, this spatial arrangement is less efficient.

It would be highly rewarding to test experimentally whether PMCA pump accumulation around the IS is indeed a necessary process for T-cell activation as predicted by our model. Unfortunately, an appropriate experimental setup appears to be hard to realize: one way would be to immobilize PMCA pumps in the PM, but they need to stay functional. Orai1, on the other hand, needs to be able to diffuse in the PM since otherwise CRAC channels would not form,

as we have demonstrated in our reaction–diffusion model for STIM1–Orai1 interaction during CRAC channel formation.

We have also studied the effect of the refilling of the ER, which usually interrupts CRAC influx by inactivation of STIM1. Again we found mitochondria position to be important for the local and global  $\text{Ca}^{2+}$  concentrations. One unexplained puzzle within the T-cell activation process is that  $\text{Ca}^{2+}$  signaling by CRAC channels is prolonged for > 1 h even though average  $\text{IP}_3$  levels (responsible for depletion of the ER) return to near basal levels within 10 min [34, 48, 49]. We were able to show within our model that cell polarization, the relocation of mitochondria and the accumulation of PMCA and SERCA pumps at the IS, can lead to an ongoing, high and robust global  $\text{Ca}^{2+}$  signal even after only a short  $\text{IP}_3$  pulse. To achieve this, (a) mitochondria have to come very close to the IS and (b) the SERCA pumps in the ER membrane must also accumulate in the vicinity of the IS. Then the mitochondria prevent  $\text{Ca}^{2+}$  not only from being extruded by PMCA pumps but also from being pumped into the ER by the SERCAs. Again it would be rewarding to test this spatial arrangement experimentally, but it provides a challenge for optical techniques since already the distance of the mitochondria to the CRAC channels is predicted to be close to the optical resolution limit ( $x_{\text{Mito}} < 300$  nm).

We found very strong dependence of the average cytosolic  $\text{Ca}^{2+}$  concentration on the distance between mitochondria at the IS and the plasma membrane (figure 8(a)). An increase of the distance between mitochondria and plasma membrane from 100 to 500 nm decreased the cytosolic  $\text{Ca}^{2+}$  concentration from about 900 to below 300 nM, a range where T-cell activation is not optimal anymore. The model predicts quite drastic cytosolic  $\text{Ca}^{2+}$  concentration changes. In fact, such  $\text{Ca}^{2+}$  changes have been observed in T-cells following the blockade of mitochondrial  $\text{Ca}^{2+}$  uptake [35, 50]; they were called  $\text{Ca}^{2+}$  transitions. These  $\text{Ca}^{2+}$  transitions may also underlie  $\text{Ca}^{2+}$  oscillations observed in T-cells. Together with altered Orai1 diffusibility as a mechanism to produce  $\text{Ca}^{2+}$  oscillations (see below), mitochondria–Orai1 channel distance regulation is a second parameter which critically influences cytosolic  $\text{Ca}^{2+}$  concentration. Additional parameters like  $\text{Ca}^{2+}$  store content [51], TRPM4 activity [52] or  $\text{Ca}^{2+}$ -activated  $\text{K}^+$  channel activity [50] may modulate  $\text{Ca}^{2+}$  oscillations but are not *per se* required for producing oscillations.

In our reaction–diffusion model for the STIM1–Orai1 interaction during CRAC channel formation, we found that negative cooperativity of STIM1 to Orai1 binding and the stabilizing effect of STIM1 already bound are essential. The model also predicts CRAC current oscillations, which would also induce oscillations of cytosolic  $\text{Ca}^{2+}$  concentration, which have been previously explained in two ways: through oscillations in  $\text{Ca}^{2+}$  store content [51] or by modulating the activity of the  $\text{Ca}^{2+}$ -activated cation channel TRPM4 [52]. Our model shows that intrinsic properties of STIM and Orai1 are sufficient to generate oscillations of cytosolic  $\text{Ca}^{2+}$  concentration; no additional feedback mechanism is required.

It is possible to combine this reaction–diffusion model to the whole cell modeling framework for spatial arrangements of organelles with respect to the CRAC channels. In particular, since we found oscillations of the CRAC current for altered diffusibility of Orai1 it would be interesting to study them in the whole cell framework as a possibility to enhance T-cell activation function [53]. Finally, we used a very simplified model for the function of mitochondria and it would be interesting to check whether physiological details of mitochondrial  $\text{Ca}^{2+}$  uptake, release, buffering and redistribution [16] add new physical features to the complex interplay of channels, pumps and organelles in T-cell polarization.



## Acknowledgments

This work was supported by the Deutsche Forschungsgemeinschaft (DFG) within the collaborative research center SFB 1027 (projects A2, A3 and C4) and the research training group GRK 1276 (HR, MP).

## References

- [1] Berridge M J, Lipp P and Bootman M D 2000 The versatility and universality of calcium signalling *Nature Rev. Mol. Cell Biol.* **1** 11–21
- [2] Roberts W M 1993 Spatial calcium buffering in saccular hair cells *Nature* **363** 74–6
- [3] Prakriya M, Solaro C R and Lingle C J 1996  $[Ca^{2+}]_i$  elevations detected by bk channels during  $Ca^{2+}$  influx and muscarine-mediated release of  $Ca^{2+}$  from intracellular stores in rat chromaffin cells *J. Neurosci.* **16** 4344–59
- [4] Cannell M B, Cheng H and Lederer W J 1995 The control of calcium release in heart muscle *Science* **268** 1045–9
- [5] Falcke M 2004 Reading the patterns in living cells: the physics of  $Ca^{2+}$  signaling *Adv. Phys.* **53** 255–440
- [6] Kummerow C, Junker C, Kruse K, Rieger H, Quintana A and Hoth M 2009 The immunological synapse controls local and global calcium signals in T lymphocytes *Immunol. Rev.* **231** 132–47
- [7] Dolmetsch R E, Pajvani U, Fife K, Spotts J M and Greenberg M E 2001 Signaling to the nucleus by an l-type calcium channel–calmodulin complex through the map kinase pathway *Science* **294** 333–9
- [8] Hoth M and Penner R 1992 Depletion of intracellular calcium stores activates a calcium current in mast cells *Nature* **355** 353–6
- [9] Zweifach A and Lewis R S 1995 Rapid inactivation of depletion-activated calcium current (ICRAC) due to local calcium feedback *J. Gen. Physiol.* **105** 209–26
- [10] Zweifach A and Lewis R S 1995 Slow calcium-dependent inactivation of depletion-activated calcium current. Store-dependent and -independent mechanisms *J. Biol. Chem.* **270** 14445–51
- [11] Shen W W, Frieden M and Demaurex N 2011 Local cytosolic  $Ca^{2+}$  elevations are required for stromal interaction molecule 1 (STIM1) de-oligomerization and termination of store-operated  $Ca^{2+}$  entry *J. Biol. Chem.* **286** 36448–59
- [12] Mullins F M, Park C Y, Dolmetsch R E and Lewis R S 2009 STIM1 and calmodulin interact with orai1 to induce  $Ca^{2+}$ -dependent inactivation of CRAC channels *Proc. Natl Acad. Sci. USA* **106** 15495–500
- [13] Derler I, Fahrner M, Muik M, Lackner B, Schindl R, Groschner K and Romanin C 2009 A  $Ca^{2+}$  release-activated  $Ca^{2+}$  (CRAC) modulatory domain (CMD) within STIM1 mediates fast  $Ca^{2+}$ -dependent inactivation of ORAI1 channels *J. Biol. Chem.* **284** 24933–8
- [14] Quintana A, Schwindling C, Wenning A S, Becherer U, Rettig J, Schwarz E C and Hoth M 2007 T-cell activation requires mitochondrial translocation to the immunological synapse *Proc. Natl Acad. Sci. USA* **104** 14418–23
- [15] Quintana A *et al* 2011 Calcium microdomains at the immunological synapse: how ORAI channels, mitochondria and calcium pumps generate local calcium signals for efficient T-cell activation *EMBO J.* **30** 3895–912
- [16] Szabadkai G and Duchen M R 2008 Mitochondria: the hub of cellular  $Ca^{2+}$  signaling *Physiology* **23** 84–94
- [17] Shuai J, Pearson J E and Parker I 2008 Modeling  $Ca^{2+}$  feedback on a single inositol 1,4,5-trisphosphate receptor and its modulation by  $Ca^{2+}$  buffers *Biophys. J.* **95** 3738–52
- [18] Rüdiger S, Nagaiah C, Warnecke G and Shuai J W 2010 Calcium domains around single and clustered  $IP_3$  receptors and their modulation by buffers *Biophys. J.* **99** 3–12
- [19] Zeller S, Rüdiger S, Engel H, Sneyd J, Warnecke G, Parker I and Falcke M 2009 Modeling of the modulation by buffers of  $Ca^{2+}$  release through clusters of  $IP_3$  receptors *Biophys. J.* **97** 992–1002
- [20] Marhl M, Schuster S and Brumen M 1998 Mitochondria as an important factor in the maintenance of constant amplitudes of cytosolic calcium oscillations *Biophys. Chem.* **71** 125–32

- [21] Grubelnik V, Zahle Larsen A, Kummer U, Folke Olsen L and Marhl M 2001 Mitochondria regulate the amplitude of simple and complex calcium oscillations *Biophys. Chem.* **94** 59–74
- [22] Schuster S, Marhl M and Höfer T 2002 Modelling of simple and complex calcium oscillations *Eur. J. Biochem.* **269** 1333–55
- [23] Zhou Y, Meraner P, Kwon H T, Machnes D, Oh-hora M, Zimmer J, Huang Y, Stura A, Rao A and Hogan P G 2009 STIM1 gates the store-operated calcium channel ORAI1 *in vitro Nature Struct. Mol. Biol.* **17** 112–6
- [24] Yuan J P, Zeng W, Dorwart M R, Choi Y J, Worley P F and Muallem S 2009 SOAR and the polybasic STIM1 domains gate and regulate orai channels *Nature Cell Biol.* **11** 337–43
- [25] Park C Y, Hoover P J, Mullins F M, Bachhawat P, Covington E D, Raunser S, Walz T, Garcia K C, Dolmetsch R E and Lewis R S 2009 STIM1 clusters and activates CRAC channels via direct binding of a cytosolic domain to Orai1 *Cell* **136** 876–90
- [26] Liou J, Fivaz M, Inoue T and Meyer T 2007 Live-cell imaging reveals sequential oligomerization and local plasma membrane targeting of stromal interaction molecule 1 after  $\text{Ca}^{2+}$  store depletion *Proc. Natl Acad. Sci. USA* **104** 9301–6
- [27] Williams R T *et al* 2001 Identification and characterization of the STIM (stromal interaction molecule) gene family: coding for a novel class of transmembrane proteins *Biochem. J.* **357** 673
- [28] Kilch T, Alansary D, Peglow M, Doerr K, Rychkov G, Rieger H, Peinelt C and Niemeyer B A 2012 Mutations of the  $\text{Ca}^{2+}$ -sensing stromal interaction molecule STIM1 regulate  $\text{Ca}^{2+}$  influx by altered oligomerization of STIM1 and by destabilization of the  $\text{Ca}^{2+}$  channel Orai1 *J. Biol. Chem.* **288** 1653–64
- [29] Gillespie D T 1976 A general method for numerically simulating the stochastic time evolution of coupled chemical reactions *J. Comput. Phys.* **22** 403–34
- [30] Gibson M A and Bruck J 2000 Efficient exact stochastic simulation of chemical systems with many species and many channels *J. Phys. Chem. A* **104** 1876–89
- [31] Teruel M N *et al* 2000 Translocation and reversible localization of signaling proteins: a dynamic future for signal transduction *Cell* **103** 181–4
- [32] Hoover P J and Lewis R S 2011 Stoichiometric requirements for trapping and gating of  $\text{Ca}^{2+}$  release-activated  $\text{Ca}^{2+}$  (CRAC) channels by stromal interaction molecule 1 (STIM1) *Proc. Natl Acad. Sci. USA* **108** 13299–304
- [33] Li Z, Liu L, Deng Y, Ji W, Du W, Xu P, Chen L and Xu T 2010 Graded activation of CRAC channel by binding of different numbers of STIM1 to Orai1 subunits *Cell Res.* **21** 305–15
- [34] Lewis R S 2001 Calcium signaling mechanisms in T lymphocytes *Annu. Rev. Immunol.* **19** 497–521
- [35] Hoth M, Fanger C M and Lewis R S 1997 Mitochondrial regulation of store-operated calcium signaling in T lymphocytes *J. Cell Biol.* **137** 633–48
- [36] Bassani J W, Bassani R A and Bers D M 1994 Relaxation in rabbit and rat cardiac cells: species-dependent differences in cellular mechanisms *J. Physiol.* **476** 279–93
- [37] Caride A J, Penheiter A R, Filoteo A G, Bajzer Z, Enyedi Á and Penniston J T 2001 The plasma membrane calcium pump displays memory of past calcium spikes *J. Biol. Chem.* **276** 39797–804
- [38] Bautista D M and Lewis R S 2004 Modulation of plasma membrane calcium-ATPase activity by local calcium microdomains near CRAC channels in human T cells *J. Physiol.* **556** 805–17
- [39] Allbritton N L, Meyer T and Stryer L 1992 Range of messenger action of calcium ion and inositol 1,4,5-trisphosphate *Science* **258** 1812–5
- [40] Verkman A S *et al* 1998 Monte Carlo analysis of obstructed diffusion in three dimensions: application to molecular diffusion in organelles *Biophys. J.* **74** 2722–30
- [41] Thul R and Falcke M 2004 Release currents of ip3 receptor channel clusters and concentration profiles *Biophys. J.* **86** 2660–73
- [42] Zhou Z and Neher E 1993 Mobile and immobile calcium buffers in bovine adrenal chromaffin cells *J. Physiol.* **469** 245–73
- [43] Berridge M J 1995 Capacitative calcium entry *Biochem. J.* **312** 1–11

- [44] Kusters J, Dernison M M, Van Meerwijk W P M, Ypey D L, Theuvenet A P R and Gielen C 2005 Stabilizing role of calcium store-dependent plasma membrane calcium channels in action-potential firing and intracellular calcium oscillations *Biophys. J.* **89** 3741–56
- [45] Torres J J, Cornelisse L N, Harks E G A, Van Meerwijk W P M, Theuvenet A P R and Ypey D L 2004 Modeling action potential generation and propagation in NRK fibroblasts *Am. J. Physiol.* **287** C851–65
- [46] Bautista D M, Hoth M and Lewis R S 2002 Enhancement of calcium signalling dynamics and stability by delayed modulation of the plasma–membrane calcium-ATPase in human T cells *J. Physiol.* **541** 877–94
- [47] Colegrove S L, Albrecht M A and Friel D D 2000 Dissection of mitochondrial  $\text{Ca}^{2+}$  uptake and release fluxes *in situ* after depolarization-evoked  $[\text{Ca}^{2+}]_i$  elevations in sympathetic neurons *J. Gen. Physiol.* **115** 351–70
- [48] Guse A H, da Silva C P, Emmrich F, Ashamu G A, Potter BV and Mayr G W 1995 Characterization of cyclic adenosine diphosphate-ribose-induced  $\text{Ca}^{2+}$  release in T lymphocyte cell lines *J. Immunol.* **155** 3353–9
- [49] Guse A H, Roth E and Emmrich F 1993 Intracellular  $\text{Ca}^{2+}$  pools in jurkat T-lymphocytes *Biochem. J.* **291** 447–51
- [50] Quintana A, Griesemer D, Schwarz E C and Hoth M 2005 Calcium-dependent activation of T-lymphocytes *Eur. Physiol. J. Pflügers Arch.* **450** 1–12
- [51] Dolmetsch R E and Lewis R S 1994 Signaling between intracellular  $\text{Ca}^{2+}$  stores and depletion-activated  $\text{Ca}^{2+}$  channels generates  $[\text{Ca}^{2+}]_i$  oscillation in T lymphocytes *J. Gen. Physiol.* **103** 365–88
- [52] Launay P, Cheng H, Srivatsan S, Penner R, Fleig A and Kinet J P 2004 TRPM4 regulates calcium oscillations after T cell activation *Science* **306** 1374–7
- [53] Dolmetsch R E, Xu K and Lewis R S 1998 Calcium oscillations increase the efficiency and specificity of gene expression *Nature* **392** 933–6